UPPSALA
UNIVERSITET

Digital Comprehensive Summaries of Uppsala Dissertations from the Faculty of Science and Technology 1799

Solution-Processable Conductive Graphene-Based Materials for Flexible Electronics

JIE ZHAO

ACTA
UNIVERSITATIS
UPSALIENSIS
UPPSALA
2019

ISSN 1651-6214
ISBN 978-91-513-0636-0
urn:nbn:se:uu:diva-381348

Dissertation presented at Uppsala University to be publicly examined in Polhemsalen, Ångströmlaboratoriet, Lägerhyddsvägen. 1, Uppsala, Wednesday, 12 June 2019 at 09:15 for the degree of Doctor of Philosophy. The examination will be conducted in English. Faculty examiner: Professor Matti Mäntysalo (Tampere University).

Abstract
Zhao, J. 2019. Solution-Processable Conductive Graphene-Based Materials for Flexible Electronics. *Digital Comprehensive Summaries of Uppsala Dissertations from the Faculty of Science and Technology* 1799. 65 pp. Uppsala: Acta Universitatis Upsaliensis. ISBN 978-91-513-0636-0.

This thesis work explores electrical conductors based on few-layer graphene flakes as an enabler for low-cost, mechanically flexible, and high-conductivity conductors in large area flexible and printed electronic devices. The flakes are deposited from aqueous solutions and processed at low temperature.

Graphene is selected for its excellent properties in mechanical, optical, electronic, and electrical aspects. However, thin films of pristine few-layer graphene flakes deposited from dispersions normally exhibit inferior electrical conductivity. One cause responsible for this problem is the loose stacking and random orientation of graphene flakes in a graphene deposition. We have solved this problem by implementing a simple post-deposition treatment leading to dramatically densified and planarized thin films. Significantly increased electrical conductivity by ~20 times is obtained. The 1-pyrenebutyric acid tetrabutylammonium salt as an exfoliation enhancer and dispersant in water yields ~110 S/m in conductivity when the graphene based thin films are processed at 90 °C. In order to achieve higher conductivity, a room-temperature method for site-selective copper electroless deposition has been developed. This method is of particular interest for the self-aligned copper deposition to the predefined graphene films. The resultant two-layer graphene/copper structure is characterized by an overall conductivity of ~7.9×10^5 S/m, an increase by ~7000 times from the template graphene films. Several electronic circuits based on the graphene/copper bilayer interconnect have been subsequently fabricated on plastic foils as proof-of-concept demonstrators. Alternatively, highly conductive composites featuring graphene flakes coated with silver nanoparticles with electrical conductivity beyond 10^6 S/m can be readily obtained at 100 °C. Moreover, a highly conductive reduced-graphene-oxide/copper hybrid hydrogel has been achieved by mixing aqueous graphene oxide solution and copper-containing Fehling's solution. The corresponding aerogel of high porosity exhibits an apparent electrical conductivity of ~430 S/m and delivers a specific capacity of ~453 mAh g^{-1} at current density of 1 A/g. The experimental results presented in this thesis show that the solution-phase, low-temperature fabrication of highly conductive graphene-based materials holds promises for flexible electronics and energy storage applications.

Keywords: Graphene, Graphene oxide, Silver, Copper, Composite, Conductive inks, Flexible electronics, Printed electronics

Jie Zhao, Department of Engineering Sciences, Solid State Electronics, Box 534, Uppsala University, SE-75121 Uppsala, Sweden.

ISSN 1651-6214
ISBN 978-91-513-0636-0
urn:nbn:se:uu:diva-381348 (http://urn.kb.se/resolve?urn=urn:nbn:se:uu:diva-381348)

To my family
献给我的家人

List of Papers

This thesis is based on the following papers, which are referred to in the text by their Roman numerals.

I **Zhao J.**, Zeng S., Wu B., Zhang S.-L., Zhang Z.-B. (2018) Re-organized graphene nanoplatelet thin films achieved by a two-step hydraulic method. *Diamond Relat. Mater.*, 84: 141–145.

II **Zhao J.**, Wen C., Sun R., Zhang S.-L., Wu B., Zhang Z.-B. (2019) A sequential process of graphene exfoliation and site-selective copper/graphene metallization enabled by multifunctional 1-pyrenebutyric acid tetrabutylammonium salt. *ACS Appl. Mater. Interfaces*, 11: 6448–6455.

III **Zhao J.**, Song M., Wen C., Majee S., Yang D., Wu B., Zhang S.-L., Zhang Z.-B. (2018) Microstructure-tunable highly conductive graphene–metal composites achieved by inkjet printing and low temperature annealing. *J. Micromech. Microeng.*, 28: 035006.

IV **Zhao J.**, Pan R., Sun R., Wen C., Zhang S.-L., Wu B., Nyholm L., Zhang Z.-B. (2019) High-conductivity reduced-graphene-oxide/copper aerogel for energy storage. *Nano Energy*, 60: 760–767.

Contributions to the papers

I Planned and performed most of the experiments apart from the SEM and XRD measurements, took part in all discussions and wrote the manuscript.

II Planned and performed most of the experiments apart from the TEM measurement, electronic circuit and low frequency filter design and measurement, took part in all discussions and wrote the manuscript.

III Planned and performed most of the experiments apart from the electronic circuit design and SEM measurement, took part in all discussions and wrote the manuscript.

IV Planned and performed most of the experiments apart from the N_2 sorption measurement, TEM measurement, EIS measurement and the corresponding data fitting, took part in all discussions and wrote the manuscript.

Publications not included in the thesis

1. Hinnemo M., **Zhao J.**, Ahlberg P., Hägglund C., Djurberg V., Scheicher R. H., Zhang S.-L., Zhang Z.-B. (2017) On monolayer formation of pyrenebutyric acid on graphene. *Langmuir*, 33: 3588–3593.

2. Song M., **Zhao J.**, Grennberg H., Zhang Z.-B. (2018) Screen printed conductive composites with reduced graphene oxide and silver. *2018 IMAPS Nordic Conference on Microelectronics Packaging (NordPac)*, 35–39.

3. Song M., **Zhao J.**, Riekehr L., Grennberg H., Zhang Z.-B. (2019) Nitrogen-doped reduced graphene oxide hydrogel achieved *via* a one-step hydrothermal process, submitted.

4. Song M., Tahershamsi L., **Zhao J.**, Zhang Z.-B., Grennberg H. (2018) Efficient gelation of graphene oxide aqueous dispersion induced by sonication-promoted Leuckart reaction. *ChemNanoMat*, 4: 1145–1152.

Contents

Abbreviations

2D	Two-dimensional
3D	Three-dimensional
GO	Graphene oxide
rGO	Reduced graphene oxide
GNPs	Graphene nanoplatelets
HMC	(Hydroxypropyl)methyl cellulose
SiC	Silicon carbide
NMP	N-methyl-2-pyrrolidone
PET	Polyethylene terephthalate
PI	Polyimide
PC	Polycarbonate
PEN	Polyethylene naphthalate
PVDF	Polyvinylidene difluoride
PU	Polyurethane
TPU	Thermoplastic polyurethanes
PDMS	Polydimethylsiloxane
DI water	Deionised water
CVD	Chemical vapor deposition
PVD	Physical vapor deposition
LED	Light-emitting diode
RFID	Radio-frequency identification
XRD	Powder X-ray diffraction
SEM	Scanning electron microscope
TEM	Transmission electron microscopy
EDS	Energy dispersive spectroscopy
SAED	Selected area electron diffraction
XPS	X-ray photoelectron spectroscopy
CV	Cyclic voltammetry
GCD	Galvanostatic charge-discharge
EIS	Electrochemical impedance spectroscopy
BET	Brunauer-Emmett-Teller
BJH	Barrett-Joyner-Halenda
PyB-TBA	1-pyrenebutyric acid tetrabutylammonium salt
NPs	Nanoparticles
PVP	Polyvinylpyrrolidone
EGaIn	Eutectic gallium-indium

PPy	Polypyrrole
PANI	Polyaniline
PAc	Polyacetylene
PTh	Polythiophenes
PEDOT	Poly(3,4-ethylenedioxythiophene)
PSS	Polystyrene sulfonate
CNTs	Carbon nanotubes
SWCNTs	Single-walled carbon nanotubes
MWCNTs	Multi-walled carbon nanotubes
ITO	Indium tin oxide

1 Introduction

Flexible electronics has been developed for around half a century and applied widely in solar cells, flexible displays, batteries, sensors, radio-frequency identification (RFID), wearable electronics and smart devices. Printing technology is employed in order to develop and additively fabricate flexible electronics of outstanding performances combined with advantages in low cost, energy efficiency and environmental friendliness. Crucial aspects toward the development of flexible and printed electronics, including the processing methods (e.g., solution-phase deposition technologies), flexible substrates and conductive materials, will be briefly discussed below.

1.1 Flexible electronics

The development of flexible electronics has been explored for around half a century across a broad range of applications including solar cells, flexible displays, batteries, sensors, RFID tags, wearable electronics and smart devices.[1-6] Compared to the conventional rigid electronics, flexible electronics exhibits the advantages of foldability, flexibility and facile interaction with humans. These advantages facilitate the widely emerging of flexible electronics and make it a competitive candidate for next generation commercial products to achieve advanced smart functions, such as electronic skin which can automatically gather biometric data about the well-being. More innovative and creative flexible electronic devices represent a development direction for future electronics.

Printing technology has been demonstrated to be highly efficient, environmentally friendly, large-area fabrication feasible and inexpensive, enabling the feasible fabrication of flexible electronics.[7] In general, photoresist, etching process and vacuum techniques can be avoided in printed electronic processes. The commonly used printing techniques (screen printing, inkjet printing, flexographic, gravure printing and aerosol jet printing) can be utilized to deposit metals, semiconductors and insulators onto a variety of substrates, such as polymeric substrates, thin glass, metal foils, metallized polymer films and paper.[8]

One of the major challenges for printed flexible electronics is to develop low-cost and high-performance conductive materials, which are important components used in all electronic devices. Metals, conductive polymers,

carbon nanomaterials and carbon/metal composites, have been developed for the realization of printed flexible conductors.[7, 9] Hybrid materials are of high interest due to their inherited advantages in all aspects by synergic effects. Meanwhile, large-area fabrication with industrialization potential is strongly needed, indicating the necessity of solution-phase deposition technologies instead of vacuum technology to produce electronic devices.[10]

Even though great advancements have been achieved over the past fifty years, flexible electronics still requires years to mature.[11] It is still hard to compete with the current semiconductor technologies. Lack of modeling, simulation and analysis tools to support design for flexible electronics is one of the roadblocks for advancement. Advancements in flexible electronics are still underway and we expect to see more of this become a reality, such as the electronic skin which can automatically gather biometric data about the well-being and the navigational map shown on the automotive glass for navigation.

1.2 Solution-phase deposition

The production of electronic devices, especially flexible devices, using solution-phase deposition shows advantages compared to competing approaches like vacuum technology based deposition. Solution-phase deposition can increase throughput and simultaneously decrease cost, which is desired in commercial manufacture. The commonly used solution-phase deposition methods include drop-casting, spin-coating, dip-coating, spray coating and the printing techniques mentioned earlier.[12] They are briefly introduced below.

Drop-casting

Drop-casting (Figure 1a) involves the process of casting solution onto a substrate and subsequent evaporation of the solvent to deposit materials of interest to form a thin film.[13] It is a very simple technique with low waste of material. However, it is limited in large area coverage and the deposition thickness is difficult to be precisely controlled. The uniformity of the deposited thin film is poor. One possible reason for the uniformity problem is the coffee ring effect, rendering a thicker edge compared to the central area.[14]

Spin-coating

Spin-coating (Figure 1b) is commonly adopted to form a thin film with relatively uniform thickness, in which a drop of solution is dropped on a substrate and then the substrate is rotated to a certain spin speed to spread the liquid and evaporate the solvent simultaneously. The thickness of the thin

film is inversely correlated to the spin speed, but also related to the viscosity and concentration of the dropped solution.[15] It possesses the advantages of good uniformity, controllability of thickness and reproducibility. But it is wasteful of materials and is not compatible with large area production. In addition, rapid evaporation of the solvent limits the time required for a well molecular ordering, which is usually translated to a good crystallization of the deposited films.[16]

Dip-coating

Dip-coating (Figure 1c) is a facile technique in which a substrate is completely immersed in a solution and then withdrawn at a controlled speed along with the evaporation of sedimentary wet coating to form a dry film.[17-19] The thickness, homogeneity and micromorphology depend on withdrawal velocity, evaporation rate of solvent, viscosity and concentration of the solution. The film achieved by dip-coating owns quite good uniformity and very thin thickness. Dip-coating possesses large area coverage by easy operation. However, the deposition is on both sides of the substrate. It also wastes material and is time consuming.

Spray coating

Spray coating (Figure 1d) is carried out by ejection of solution droplets from nozzles. The small droplets are formed through aerosolization. A thin film can be achieved by merging wet droplets into a full wet film on substrate and then drying, or droplets drying independently on substrate. A rougher film is obtained in the latter case, but wettability issue can be avoided wherein due to the absence of forming full wet film. The size and shape of spray nozzle, the atomizing gas pressure, as well as the concentration, viscosity and surface tension of the deposited solution influence the quality of spray coating.[20] Spray coating is roll-to-roll compatible and suitable to various substrates with large area coverage.[21-22]

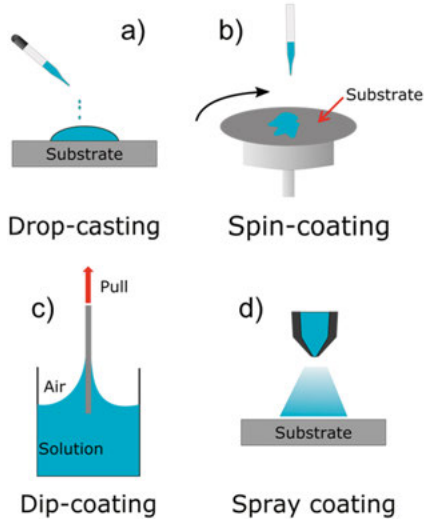

Figure 1. Schematic illustration of a) drop-casting; b) spin-coating; c) dip-coating; d) spray costing.

Printing

Printing techniques can be divided into contact printing and non-contact printing, depending on whether there is a directly physical contact between the printing equipment and the substrate or not during the ink transferring onto the substrate.[10] Contact printing includes screen printing, flexography and gravure printing, while non-contact printing includes aerosol jet printing and inkjet printing.

Screen printing

Screen printing can be performed in a planar (Figure 2a) or roll-to-roll manner, in which ink is squeezed by a blade through a screen mesh onto a substrate along with defining a designed pattern.[7] Screen printing is a simple and mature technique which is suitable for paste-like inks with high viscosity (0.1 to 10 Pa·s).[23] And the thickness of achieved film typically ranges from several tens to a few hundred micrometers. However, the resolution is limited to the level of ~50 to 150 μm[24] and ink is wasteful during the printing. In addition, the speed of the planar system is relatively low compared with the other conventional printing techniques.[23]

Flexography and gravure printing

Flexography (Figure 2b) is a letterpress printing technology, in which quick-drying and semiliquid ink is used. It is a roll-to-roll direct printing technique

and a high speed printing process. However, due to the Halo effect that may occur during the printing, a low resolution and instability of pattern size that leads to smudge or lumpy pattern are expected.[23]

Gravure printing (Figure 2c) involves the process of transferring ink into the grooves of the gravure and being followed by picking up the ink onto a substrate.[25] It is a high speed and high quality printing technique with high throughput, uniformity and long print runs.[26] There are several parameters, including ink properties (viscosity of the ink and evaporation rate of the solvent), proper cell spacing, shear force on ink transferring, that affect the quality of the printed patterns.[27-28] Changes in the patterns for both flexography and gravure printing techniques require a redesign of printing rolls, which is both time-consuming and expensive.

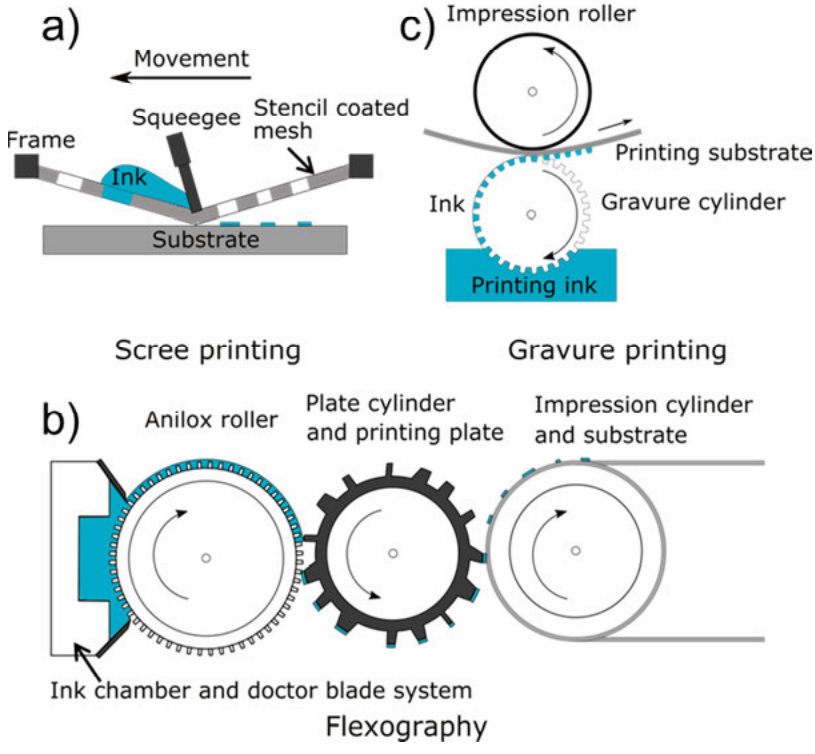

Figure 2. Schematic illustration of a) screen printing performed in a planar manner; b) flexography; c) gravure printing.[23, 29]

Aerosol jet printing

Aerosol jet printing (Figure 3a) is a direct write technique for manufacturing patterns on a substrate. The ink is aerosolized and delivered to the substrate by carrier and sheath gas.[30-31] It works at low temperature, which allows the utilization of many materials and substrates. Aerosol jet printing can be also applied for irregular three-dimensional (3D) surfaces and complex geome-

tries since the distance between the nozzle and the substrate is controllable.[32] It can be used in the manufacture of flexible displays, high efficiency solar cells, sensors, resistors, printed antennae, printed transistors, and so on. But there are still some challenges, such as lowered quality caused by carrier and sheath gas. The flow rate of the carrier and the sheath gas, as well as the speed of the stage, influences the quality of the printed patterns.[33]

Inkjet printing

Inkjet printing (Figure 3b) has been extensively explored by both commercial and scientific communities. A desired pattern can be printed directly on a substrate from a digital format stored in a computer. It involves ejection of ink from a nozzle and subsequent deposition of the ink droplet onto a substrate.[12] The viscosity and surface tension of the ink, as well as the surface energy of the substrate are important parameters in inkjet printing. It is necessary to balance the processing parameters to precisely control the fluid momentum transfer and droplet spread.[34-35] Drying of the droplet on a substrate is just similar to that in a normal drop-casting. It is a low material wastage and environmentally friendly method. The viscosity of the ink is in the range of ~1-10 mPa·s and surface tension ranges from ~20 to 70 mN/m.[36-37] The achieved thickness of the printed films is usually up to a few hundreds of nanometer at most and the reliable feature resolution is limited to ~15-20 μm for a high throughput production.[10, 38] In general, the printing speed is low in comparison with the other printing techniques and the nozzle is easy to be clogged during the printing, which are the challenges in inkjet printing.

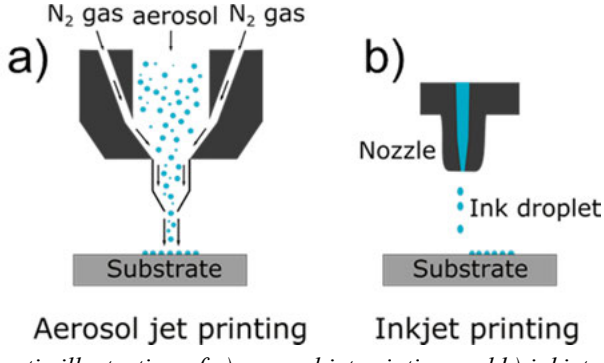

Figure 3. Schematic illustration of a) aerosol jet printing and b) inkjet printing.

1.3 Substrates in flexible electronics

Substrates play an important role in the development of flexible electronics. The most used substrate materials include polymeric substrates, thin glass,

metal foils, metallized polymer films and paper.[38-46] Each kind of substrate has its specific benefits and could be used to fulfill specific requirements. The selection of substrates strongly depends on their properties, such as electrical and thermal conductivity, thermal deformation, optical transmittance, mechanical flexibility, solvent resistance and the compatibility with the deposited materials and the processing steps to be used.

Polymeric substrates

Polymeric substrates are the most commonly used ones in flexible electronics due to their low cost, robustness to deformation and large freedom in design. Polyimide (PI), polycarbonate (PC), polyethylene naphthalate (PEN), polyethylene terephthalate (PET), polyvinylidene difluoride (PVDF), polydimethylsiloxane (PDMS), polyurethane (PU) and thermoplastic polyurethanes (TPU) are the mainly used polymeric substrates.[39, 47-54] The maximum processing temperature of polymeric substrates is typically limited to several hundred degrees Celsius according to the glass transition point of the substractes.[40, 55] Meanwhile, additional barrier coating is necessary in some applications because of the inferior hermeticity. The purpose of this is to strictly exclude water and/or oxygen.[56] Prior surface treatments are usually required before the fabrication due to their low surface energy. Compared with glass or metal, the Young's moduli of most polymeric substrates are much lower.

Table 1. The comparison of the different polymeric substrates and glass substrate.[7]

Substrate	PI	PC	PEN	PET	PVDF	PDMS	PU	TPU	Glass
Glass transition temperature (°C)	155–270	145	120–155	70–110	–39	−125	–	80	–
Melting temperature (°C)	250–452	115–160	269	115–258	156–165	–	–	180	1400–1600
Density (g/cm^3)	1.36–1.43	1.20–1.22	1.36	1.39	1.77–1.80	1.03	1.2	1.18	2–8
Solvent resistance	Good	Poor	Good	Good	Good	Poor	Fair	Good	Good
Water absorption (%)	1.3–3.0	0.16–0.35	0.3–0.4	0.4–0.6	< 0.10	> 0.1	0.1	0.2	0.3
Coefficient of thermal expansion (ppm/°C)	8–20	75	20	15–33	80–140	250–300	–	153	8–30
Work temperature (°C)	Up to 400	Up to 130	Up to 155	Up to 150	Up to 150	Up to 200	–	Up to 130	Up to 1000
Dimensional stability	Fair	Fair	Good	Good	Good	Good	Good	Good	Fair
Volume resistivity (Ω·cm)	1.5×10^{17}	10^{12}–10^{14}	10^{5}	1.0×10^{19}	10^{14}	1.2×10^{14}	–	3.0×10^{14}	10^{16}

Glass substrates

Both glass and polymeric substrates can be optically transparent, which enables them to be applied in optoelectronic applications. Especially for glass, it has a wide optical window. The flexible glass substrates have been used in the area of thin-film transistor, lighting, displays, touch sensors and photovoltaics due to the high-quality surface, optical transmission, hermetic barrier property, thermal capability, dimensional stability and chemical compati-

bility.[41, 57-59] Flexible glass is also compatible with sheet and continuous processing such as roll-to-roll fabrication. However, the glass substrates are fragile prone to breaking when being bent too much. And the broken glass generates fragments which may induce particle contamination.[41]

Metal foils and paper substrates

Metal foils are compatible with high temperature fabrication. They show high electrical conductivity, good stability against stretching and excellent hermetic barrier property comparable with polymeric substrates. However, metal foils are readily to form irreparably wrinkle, which will influence the performance of the fabricated devices involving web handling.[10] High cost and the restriction on the freedom of design limit their wide applications.

Paper substrates are environment-friendly and easy to be folded and unfolded. Paper electronic devices have attracted lots of interests due to the low cost and recyclability of paper. Various electronic devices, such as capacitor, batteries and smart cards, have been fabricated on paper or paper-like substrates.[60-61] However, due to the porosity of paper substrates, their application in printed electronics, which need high hermetic barrier property, is limited.[10]

1.4 Compatibility between deposited materials and substrates

The properties of both substrate and deposited solution could influence the interfacial wettability and adhesion.[7] Good wettability indicates that the liquid spreads evenly over the surface of substrate without forming droplet. Contact angle (θ), which measures the angle between the solid-liquid interface and the liquid-vapor interface, is used to determine the wettability of liquid on the surface of a substrate.[62] The interrelation of contact angle and the interface energy between the solid and vapor (γ_{sv}), the interface energy between the solid and the liquid (γ_{sl}), and the interface energy between the liquid and vapor (γ_{lv}) follows Young's equation:

$$\gamma_{sv} - \gamma_{sl} - \gamma_{lv} \cos\theta = 0 \tag{1.1}$$

As shown in Figure 4, a liquid drop completely wets the substrate when θ = 0°, while it does not wet the substrate at all when θ = 180°. Liquid is easier to spread evenly over the surface if 0° < θ < 90° and the substrate surface is considered hydrophilic, while liquid tends to form droplet if 90° < θ < 180° and the substrate surface is considered hydrophobic.

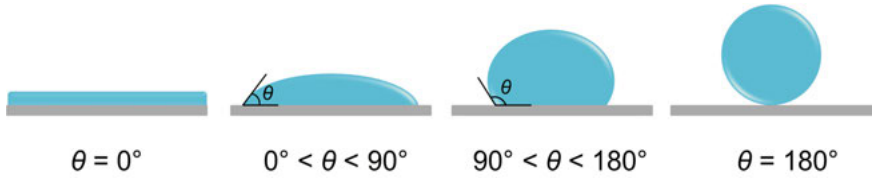

Figure 4. Liquid drop on substrate surface with different contact angles.

Many factors determine the adhesion between deposited materials and substrate coherently, for example, the chemical and physical forces at the interface. Specifically, the factors contain chemical composition, functional groups, porosity and surface morphology of the substrate; chemical composition, evaporation rate of solvent and rheological behavior of the deposited solution. Substrates like metal and glass are normally of high surface energy and most polymeric substrates are of low surface energy. The adhesion can be enhanced by chemical treatment, surface roughness enhancement, flame treatment, corona discharge and plasma treatment.[54, 63-65] Flame and plasma treatments can realize surface cleaning and also create functional groups on the surface to change its surface energy. However, the hydrophobic property could recover if the substrate is exposed to air for a long time.[66] The chemical treatment can adjust both the chemical and physical properties of the substrate surface to improve the interactions between the deposited material and the substrate.[67]

1.5 Conductive materials in printed electronics

With the advancements of flexible electronics, printed electronics of low cost, environmental friendliness and flexibility have attracted tremendous interests.[68-69] Many factors (such as materials and manufacturing processes) determine the progress of printed electronics, in which the fabrication of low cost and environmentally friendly conductive inks is the crucial one. In electronic circuits, interconnect structures are one of the most important part concerning the overall chip performance. The *RC* time delay of a signal propagating along a line is approximately equal to $0.89RC$, where R is the line resistance and C is the total capacitance associated with the line.[70] Lower resistance of the line can provide shorter time delay in circuits. Hence, fabricating highly conductive interconnect structures is crucial in printed electronics. The most used conductive inks include metals, conductive polymers, carbon nanomaterials and carbon/metal composites.

1.5.1 Metals

Metals, such as Ag ($\sigma = 6.3 \times 10^7$ S/m), Cu ($\sigma = 5.96 \times 10^7$ S/m), Al ($\sigma = 3.78 \times 10^7$ S/m), Ni ($\sigma = 1.43 \times 10^7$ S/m) and Au ($\sigma = 4.42 \times 10^7$ S/m), ex-

hibit excellent conductivity acting as the connection component in the electronic devices. It is the primary advantage for metals to be used as conductive inks. Metal-based conductive inks normally employ metal nanoparticles dispersed in liquid, metal organic decomposition and liquid metal.[71-74] Melting temperature of metal nanoparticles is much lower than that in bulk materials, especially in the case when the particle diameter is below 100 nm. This property makes it possible to sinter metal nanoparticles at a relative low temperature in printed electronics.[75-77] Silver is widely used and frequently reported for conductive ink since it possesses high conductivity, easy preparation and resistance to oxidation.[78-79] Silver nanoparticle inks have been already commercially available. However, the cost of silver inks is high. Compared with silver, copper is much cheaper and its conductivity is close to silver, which makes it an alternative ink filler.[80] However, copper is easy to be oxidized when it is exposed in ambient atmosphere particularly at nanoscale in size and its oxide is non-conductive. It is necessary to prevent copper from oxidation, which needs an additional step and complicates the fabrication process.[81] Gold and platinum are expensive materials which will result in the elevated cost of the inks.[78] The other metals (such as nickel, tin, iron and aluminum) can also be used in conductive inks, but they all suffer from oxidation as copper.

The preparation of metal nanoparticles can be divided into two categories, i.e. chemical method and physical method. The chemical method includes liquid phase reduction, decomposition of precursor and electrochemical method, while the physical method is associated with the transition of bulk materials into nanoparticles followed by the dispersion of the nanoparticles in some appropriate media.[82-86] In order to extend the shelf time of metal nanoparticles used as conductive ink, it is necessary to guarantee the dispensability and to prevent inks from oxidizing. Adding proper stabilizer is an efficient way to avoid the agglomeration of metal nanoparticles. Polyvinylpyrrolidone (PVP), which owns both hydrophobic and hydrophilic groups and can simultaneously interact with metal nanoparticles and the dispersion medium, is one of such polymer surfactant stabilizers. It is a common approach to employ PVP with different molecular weight to formulate the inks of silver or copper.[76, 87] The conductive inks formulated by metal nanoparticles need a subsequent post-treatment (e.g., annealing) for sintering the nanoparticles to make the ink deposited on a substrate highly conductive.

Liquid metal is a potential candidate for conductive ink since it possesses intrinsically high conductivity (~10^6 S/m). It is a kind of metal that is in liquid phase at room temperature and superior to many other liquid materials in the aspect of electrical and thermal conductivity at low temperature.[72] For instance, the eutectic gallium indium alloy (EGaIn) and GaInSn exhibit low toxicity, low melting point and high electrical conductivity (~3.4×10^6 S/m for EGaIn and ~3.5×10^6 S/m for GaInSn), making them attractive in flexible electronics.[88]

1.5.2 Conductive polymers

Conductive polymers have attracted much attention due to their excellent solution-phase processability, mechanical flexibility and light-weight. The solution-processible organic compounds can avoid time consuming and high cost of vacuum fabrication processes. In addition, they exhibit good mechanical stability and adhesion on flexible plastic substrates even under bending conditions because of the organic nature. However, their shortcomings cannot be overlooked, such as low conductivity which may lower the performance of electronic devices.[89] The conductivity of solution-processable conductive polymers ranges from very low values up to the value of ~10^4 S/m (Figure 5).[90]

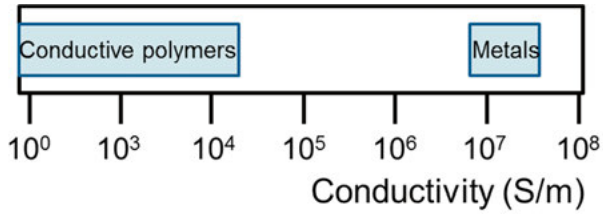

Figure 5. The range of conductivity of conductive polymers and bulk metals.

The development of organic electronics based on conducting polymers was triggered since the discovery of polyacetylene by Macdiarmid *et al.* in 1977.[91] Polypyrrole (PPy), polyaniline (PANI), polyacetylene (PAc) and polythiophenes (PTh) are the most common conductive polymers (Figure 6). In addition, poly(3,4-ethylenedioxythiophene) (PEDOT), which is formed by polymerization of bicyclic monomer 3,4-ethylenedioxythiophene, is also one of the promising conductive materials due to its versatile processability, high electrical conductivity, good chemical and air stability. Polystyrene sulfonate (PSS) is usually added to the aqueous PEDOT solution to increase the stability of the dispersion.[92] Conductive polymers have been used in various fields like displays, transistors, wearable electronics and sensors. Several examples are worth to noting, such as the application of PANI nanofiber ink in sensors, circuit and conducting films by inkjet printing,[93] the employment of PPy to produce chemiresistor sensors through inkjet printing,[94] the fabrication of transparent and flexible PEDOT:PSS/PANI electrodes using inkjet printing.[89]

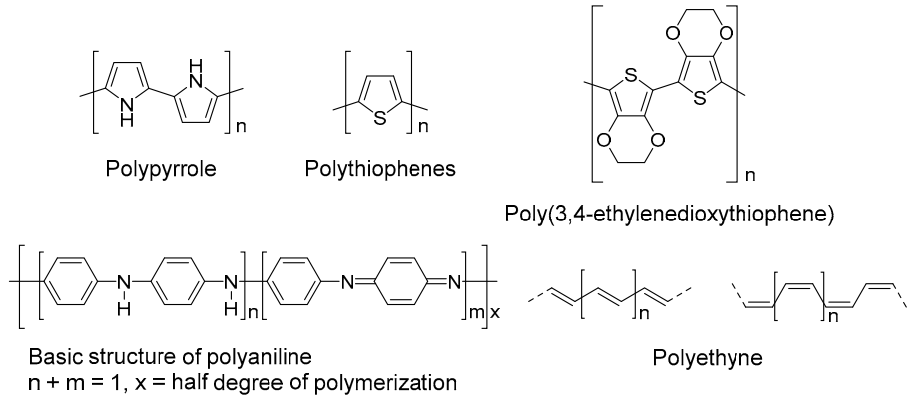

Figure 6. The structural formula of polypyrrole, polythiophenes, poly(3,4-ethylenedioxythiophene), polyaniline and polyacetylene.

1.5.3 Carbon nanomaterials

Carbon nanotubes and graphene are two major carbon allotropes. They own high electron mobility, high conductivity, outstanding optical property, chemical stability, high mechanical flexibility, which make them promising competitive conductive materials in flexible electronics.[95-98]

Carbon nanotubes

Carbon nanotubes (CNTs) are cylindrical hollow nanostructures with walls composed of seamless rolled-up one or more layers of carbon atoms in hexagonal lattice, referring to single-walled carbon nanotubes (SWCNTs) or multi-walled carbon nanotubes (MWCNTs), respectively. The typical diameter ranges from 0.8 to 2 nm for SWCNTs and from 5 to 20 nm for MWCNTs. Their lengths are from less than 100 nm to several centimeters.[97] The intrinsic electrical conductivity of individual CNTs is ~10^8 S/m for SWCNT and ~10^7 S/m for MWCNT. But the value is much lower in most practical cases because of the formation of different defects or impurities during the synthesis.[95] A thin film formed with CNTs shows good mechanical properties of stretchability and flexibility due to the superior mechanical properties of individual CNTs and the network structure of the CNT film.

The advantageous electrical and mechanical properties make CNTs a promising candidate for printed electronics. However, poor inter-tube contact among the individual CNTs in printed patterns results in high contact resistance. In addition, aggregation of CNTs due to the van der Waals interaction is a major challenge for the formulation of CNT inks. Aggregated CNTs easily clog nozzles in inkjet printing. There are several approaches for achieving stable CNT dispersions depending on the hydrophobic property of CNTs, including dispersion of CNTs in organic solvent without/with stabi-

lizer, dispersion of CNTs in aqueous solution in the presence of proper stabilizer, modification of CNTs by chemical method to enhance the interactions with the dispersion medium.[96] In order to obtain the homogeneous CNT dispersion, certain energy must be injected to break the aggregation of CNTs and this can be implemented by means of long-time ultra-sonication, high-shear mixing, ball milling and high pressure homogenization.[95]

CNTs have been utilized in various applications, in which transparent electrode is one of the most interesting applications.[96] CNTs could provide a cheaper alternative compared with the commercial indium tin oxide (ITO). Screen printing, inkjet printing and aerosol jet printing are commonly used for CNT deposition on different substrates.[99] For example, high-performance carbon nanotube transparent conductive films are achieved by inkjet printing employing "coffee ring effect".[100] The obtained films of sheet resistance of 156 Ω/□ and transparency of 81% at 600 nm after post-printing treatment with hot nitric acid have been demonstrated.

Graphene

Graphene, a two-dimensional (2D) monolayer of sp^2 bonded carbon atoms arranged in a honeycomb lattice, has attracted considerable scientific attention in recent years due to the unique electronic, mechanical and thermal properties, as well as the property of high surface area.[98, 101-103] It has wide potential applications for transparent conductive films, sensors, transistors, catalyst supports and energy storage devices.[104-106]

Various approaches can be used for production of graphene and each one has its pros and cons. The commonly used approaches include chemical vapor deposition (CVD), mechanical cleavage, liquid-phase exfoliation, reduction of graphene oxide, annealing of silicon carbide (SiC) and molecular assembly. CVD graphene can be produced in roll-to-roll manner to achieve infinite size and be easy to obtain one layer graphene with few defects.[107-108] However, CVD graphene is polycrystalline and needs to be transferred to desired substrates (insulator or semiconductor substrate) from its growth metal substrate (such as Cu) firstly for the following processes in applications, during which the graphene could be contaminated and destroyed. Mechanical cleavage ("mechanical exfoliation" in Figure 7) provides the highest quality and cleanest graphene, while the quantity is low and size is also limited.[109] Both liquid-phase exfoliation and reduction of graphene oxide exhibit mass scalable and cost effective. Liquid-phase exfoliation utilizes physical forces, such as ultra-sonication and shear mixing, to exfoliate graphene sheets from pristine graphite.[110-111] In general, the achieved graphene sheets can be few-layer with few defects. But it is difficult to obtain large size and single layer graphene. The pristine mono- and few-layer graphene sheets are not dispersible in most solvents including water. Stabilizer is a must to achieve stable graphene dispersions. But most stabilizers in use are

non-conductive which degrade the conductivity of the obtained graphene thin films. Production of graphene flakes *via* oxidation and reduction process, which yield reduced graphene oxide (rGO), is highly scalable.[112] This production method however suffers from high density of defects in the graphene. SiC graphene is grown directly on semiconductor substrate and can be controlled to form single layer.[113] Nevertheless, some carbon atoms binding to Si by covalent bonds results in defects in graphene and this method is also too expensive to use in large scale.[114] We mainly focus on shear mixing for production of graphene, considering that it is inexpensive, scalable and easy to be used in flexible electronics.

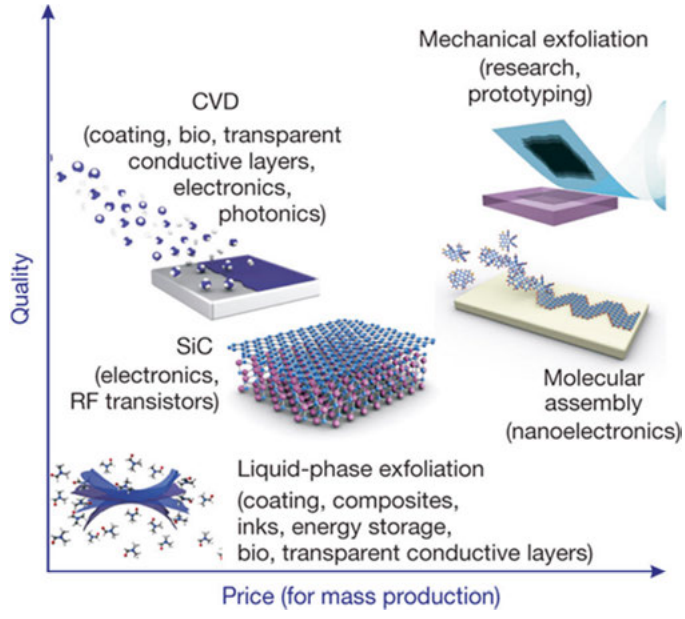

Figure 7. Different methods for production of graphene, and their corresponding size, quality, price, as well as applications. Reprinted with permission from [109]. Copyright (2012) Springer Nature.

Since pristine graphene is hydrophobic, it is necessary to functionalize its surface, e.g., by applying proper stabilizer, to disperse graphene in aqueous solution. In order to utilize graphene dispersion in printing technology, adjustment of the rheological properties of the dispersion is necessary for ink formulation. There are several requirements for graphene based inks, including proper viscosity and surface tension (1-25 mPa·s and 25-50 mN/m, respectively, for inkjet printing),[115] stable dispersion without aggregation and precipitation, simple synthesis procedure, good adhesion of deposited fillers to substrate and good conductivity of the achieved patterns. Hotplate and oven are the most used methods for thermal annealing in lab. Sometimes in order to remove the non-conductive stabilizer, the annealing temperature at

or higher than 300 °C is required. However, the high annealing temperature is not compatible with most of the polymeric substrates.

The formulation of stable graphene inks can be achieved from pristine graphene with appropriate stabilizer or GO without the need of stabilizer. The most used stabilizers contain surfactants, ethyl cellulose, polymers, polycyclic aromatic hydrocarbons and ionic liquid. Both water and organic solvent (such as N-methyl-2-pyrrolidone (NMP), dimethyl sulfoxide, ethanol, terpineol and dimethylformamide) are employed to disperse graphene.[116]

Ferrari *et al.* reported a fabrication method for large-area graphene devices using inkjet printing, in which the graphene-based ink is produced through liquid phase exfoliation of graphite in NMP.[117] The printed thin film transistors possess mobilities up to ~95 $cm^2V^{-1}s^{-1}$ and show a combination of transmittance of ~80% and sheet resistance of ~30 kΩ/□. However, NMP is not environmentally friendly and better to be avoided in printing process. Hersam *et al.* developed a graphene ink based on graphene/ethyl cellulose powder to achieve stable inkjet-printed features on various substrates.[118] The graphene ink is prepared by exfoliation of graphite in the presence of ethyl cellulose in ethanol. The inkjet-printed graphene features exhibit uniform morphology with conductivity of 2.5×10^4 S/m after thermal annealing at 250 °C for 30 min. They are also compatible with flexible substrates and show outstanding tolerance to bending stresses. However, the presence of the salt-induced flocculation and redispersion of graphene/ethyl cellulose leads to a complicated procedure and limits the commercial application. Friedrich *et al.* described the gelation of highly concentrated graphene/polymer dispersions and utilization of the inks in screen printing.[119] The printed features show conductivity of 1.3×10^3 S/m only by drying at 100 °C for 5 min, which has potentials in roll-to-roll applications of printed flexible electronics.

1.5.4 Graphene/metal composites

Production and properties of graphene/metal composites largely depend on mass scalable production of graphene and homogenous dispersion of graphene flakes and metal ions/nanoparticles. Both of these two parts are crucial for achieving a graphene/metal composite with improved properties for the applications.[120] Graphene/metal hybrid inks have attracted great interest in recent years.[121-125] The hybrid inks could inherit advantages of both graphene and metal, e.g., enhanced conductivity of a resultant graphene/metal composite film compared to a graphene film alone and lowered cost due to reduction of the use of metal, particularly, precious metal providing that the cost of graphene production becomes cheap enough. In addition, the incorporation of graphene to the composites is expected to enhance the specific strength and thermal conductivity.[126]

In general, graphene/metal composites are obtained by mixing graphene nanosheets together with metal nanoparticles, in which the most studied one is graphene/silver composites. The reason is that silver inks are more cost effective in comparison with palladium and gold based inks and are more chemical stable than copper inks.[78]

Han *et al.* reported a Ag-graphene hybrid ink for electronics on paper.[124] The deposited Ag nanoparticles on the surface of graphene sheets decrease the contact resistance of graphene junctions and the presence of graphene builds efficient electrical pathways between the aggregated Ag nanoparticles to reduce the negative influence of voids. The resulting conductivity is ~5.3 $\times$ 10^6 S/m after curing at 100 °C. The conductivity of the tested pattern is only decreased slightly even over thousands of bending cycles or rolling. Song *et al.* fabricated highly conductive transparent patterns with a Ag nanotriangle platelet-rGO (Ag NTP-rGO) hybrid ink, in which pure water is used as solvent.[122] Monodispersed Ag nanotriangle platelets (Ag NTPs) can be self-assembled on GO, in which GO can be used as both dispersant and stabilizer. The resultant Ag NTP-rGO patterns exhibit low sheet resistance of 170 Ω/□ and transparency of 90.2% after reduction by means of long thermal treatment (110 °C for 3h in a vacuum oven). Gao *et al.* synthesized a dispersed Ag/rGO composite by anchoring silver nanoparticles (Ag NPs) on the surface of rGO.[125] The Ag/rGO composite acting as a conductive ink filler shows good dispersibility. Ag NPs could serve as nanoscale spacers to avoid the agglomeration of rGO and nozzle jam. The conductivity of the Ag/rGO filler could be controlled by changing the reaction time. The inkjet-printed patterns exhibit an optimum conductivity of 2 $\times$ 10^3 S/m.

1.6 Challenges in solution-phase processable graphene based materials

Electrical conductivity is a primary figure of merit of conductive graphene films. For the applications of interconnects, electrical conductivity determines the speed of circuits. Electrical conductivity of solution-phase deposited graphene thin films to a large degree depends on the organization of the individual graphene flakes and the type of stabilizer in use. The former influences inter-flake contacts and it remains a challenge to control the flake orientation in graphene thin films. This is also a general issue for other 2D materials. The latter is a severe problem when low temperature is preferred and even required for temperature-sensitive substrates. For instance, processing temperature lower than 100 °C is safe for cellulose based substrates. Printed graphene/metal composite is a promising solution towards additive manufacturing of highly conductive features. But so far most of the studied materials suffer from either high temperature annealing or complicated pro-

cessing steps. Further research effort is needed for solution-phase and low-temperature processable graphene based materials that are cost-efficient and of high performance, which motives this thesis work.

2 Scope of the thesis

The aim of this thesis is to develop and study highly conductive materials with few-layer graphene flakes as a key component, with deposition from aqueous solution and low temperature processing. This work is mainly motivated by the demands for low-cost, mechanically flexible, and highly conductive conductors as interconnects in additive manufacturing of large area printed and flexible electronic devices.

Graphene has been selected as the key component in the preparation of new conductive materials due to its ultrahigh surface area, chemical inertness and excellent properties in mechanical, optical, electronic and electrical respects. However, thin films of pristine few-layer graphene flakes deposited from dispersions normally stack loosely with random orientation, which seriously limits their electrical conductivity. Additionally, the presence of polymeric dispersant used in exfoliation and dispersion of graphene leads to further degrading of the electrical conductivity unless annealing at high temperature is applied. **Paper I** presents a post-deposition treatment method to former problem. Individual graphene flakes were efficiently re-oriented in as-deposited films and thus dramatically reduced the inter-flake contact resistance. Densified, smoothened and homogenized graphene thin films with increased electrical conductivity can be readily achieved as a result. The method developed is universally applicable to solution-phase deposition of other 2D materials.

To solve the problem associated with polymeric dispersant, **Paper II** utilizes a small molecular 1-pyrenebutyric acid tetrabutylammonium salt (PyB-TBA) as exfoliation enhancer and dispersant in water. With PyB-TBA, conductive graphene thin films with ~110 S/m are achieved when drying is performed at 90 °C. In order to further increase the electrical conductivity of graphene films for interconnect applications, a novel room-temperature method of site-selective copper electroless deposition that is self-aligned to the predefined graphene films has been developed, leading to a two-layer graphene/Cu structure with conductivity of ~7.9×10^5 S/m. Demo circuits on plastic foils have been fabricated based on the developed technique showing a great potential for application in flexible devices.

Alternatively, as **Paper III** reports, further conductivity enhancement can be realized by composites. For this purpose, hybrid inks were prepared by mixing pristine few-layer graphene dispersion and reactive silver solution at different volume ratios in aqueous phase. Highly conductive and morpholo-

gy-tunable graphene/Ag composite films on various substrates have been readily obtained by inkjet printing with processing temperature 100 °C at the most. The availability of graphene/Ag composite films can pave the way to the metallization in a variety of printed devices.

As graphene oxides are cheap and highly dispersible in aqueous media, an attempt to prepare hybrid ink with aqueous graphene oxide solution and copper-contained Fehling's solution has been conducted. Unexpectedly, macro-assembling in the solution occurs at room temperature, leading to a formation of highly conductive rGO/copper hybrid (Cu/Cu_xO@rGO) hydrogel as described in **Paper IV**. A subsequent freeze-drying of the hydrogel leads to aerogel. The aerogel of rGO networks decorated with Cu/Cu_xO nanoparticles show apparent electrical conductivity of ~33 S/m and ~430 S/m prior to and post mechanically compression. The compressed Cu/Cu_xO@rGO aerogel electrode delivers a specific capacity of ~453 mAh g^{-1} at a current density of 1 A/g, indicating a great potential application in the area of energy storage.

3 Material preparation and characterization methods

The aim of this thesis is to develop and study conductors containing few-layer graphene flakes as key component deposited from aqueous solutions and processed at low temperature. Aqueous graphene dispersion is obtained by liquid-phase shear exfoliation of graphite in DI water. Conductive graphene/metal hybrid materials are achieved by employing the reactive silver solution or electroless deposition of copper. So, shear exfoliation, inkjet printing, modified Tollens' process and electroless deposition used for material preparation are briefly discussed in this chapter. Characterization techniques used in Paper I to Paper IV are also presented.

3.1 Shear exfoliation

Shear exfoliation is a solution-phase method to prepare 2D materials from their bulk stack state, such as graphene from graphite. It provides a scalable method for producing large quantities of defect-free pristine graphene sheets in both organic solvent (such as NMP) and aqueous solution with certain stabilizers.[110]

The mixer used in this thesis is a L5M high shear laboratory mixer, made by Silverson (Figure 8). The mixing work-head consists of a rotor with four blades and a screen known as the stator, as shown in Figure 8. The rotor locates within a fixed screen. The working principle includes four stages. Firstly, the high-speed rotation of the rotor blades generates a powerful suction, drawing liquid together with the dispersed solid materials upwards into the center of the work-head. Secondly, the materials move towards the periphery of the work-head under centrifugal force, during which the materials suffer a milling action in the clearance between the ends of the rotor blades and the inner wall of the stator. Thirdly, the materials are forced to go out through the perforations in the stator and circulated in the mixture with high velocity undergoing intense hydraulic shear. Finally, the fresh materials are continually drawn into the work-head along with the expelling of the materials from the head to maintain the mixing cycle. The concentration of produced graphene is related to the processing parameters: rotor diameter, initial graphite concentration, mixing time, liquid volume, rotor speed.

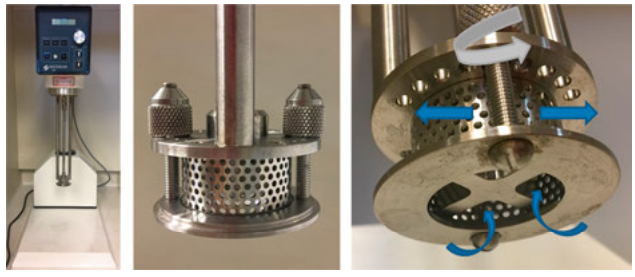

Figure 8. The photographs of the Silverson model L5M high-shear mixer (left) and close up view of the work-head (middle and right). The top arrow (grey one) in the right image shows the direction of rotation and the other groups of arrows (blue ones) reveal the direction of liquid flow.

According to the literature,[110] turbulent energy dissipation is known unnecessary during the production of graphene by shear exfoliation. Graphene can be also produced when the Reynolds number (*Re*) is below 10^4, where turbulence is not fully developed.[127] In the hydrodynamic system, the Reynolds number is usually used as a criterion to judge the appearance of turbulence, which is defined as:

$$Re = \frac{ND^2\rho}{\eta} \tag{3.1}$$

where N and D are rotor speed (in rpm, 1 rpm = $2\pi/60$ rad/s) and rotor diameter (in m), respectively; ρ and η are liquid density (in g/cm^3) and viscosity (in Pa·s), respectively.

A minimum requirement on shear rate ($\dot{\gamma}_{min}$, the unit is s^{-1}) is needed during shear exfoliation. Shear rate ($\dot{\gamma}$) can be calculated by the following equation:

$$\dot{\gamma} \approx \frac{\pi ND}{\Delta R} \tag{3.2}$$

where ΔR is the rotor-stator gap (in m).

According to the literature,[110, 128] $\dot{\gamma}_{min}$ can be predicted if the exfoliation is modeled as shear-induced interlayer sliding in a solvent, through:

$$\dot{\gamma}_{min} = \frac{\left(E_{S,G}^{1/2} - E_{S,L}^{1/2}\right)^2}{\eta L} \tag{3.3}$$

where $E_{S,G}$ and $E_{S,L}$ are the surface energy (in J/m^2) of graphene and liquid, respectively; L is the length of exfoliated flake (in m). This equation clearly reveals that the exfoliation energy is minimized when the surface energy of solvent approaching that of graphene. It has been demonstrated that NMP,

which exhibits the surface energy of 69 mJ/m^2,[111] can facilitate shear exfoliation at a low shear rate. We can observe that lower shear rate leads to larger flake size.

In typical experiments, the mixture of graphite and solvent are added into the mixing vessel and the work-head is then lowered and positioned in the middle of the vessel. A working time is set and the speed is gradually increased to a desired value. In order to prevent heating the mixture during long time running, the vessel should be bathed in water with recirculation. In this thesis, the speed of shear mixing was 5000 rpm and the processing time was 20-30 min.

3.2 Inkjet printing

Inkjet printing creates designed patterns by propelling droplets of inks onto a substrate. This printing technology was first developed in the early 1950s. It has been intensively studied in the field of printed electronics. Compared to screen printing, also a common method in printed electronics, inkjet printing gives thinner printed layers and a higher resolution. However, the dynamic viscosity of inks is more restricted, ranging from 1 to 10 mPa·s. Based on the mechanism of droplet generation, inkjet printing could be divided into two categories, i.e. continuous inkjet and drop-on-demand inkjet.[35] The drop-on-demand inkjet possesses simpler system than continuous inkjet. The thermal inkjet, piezo inkjet, as well as electrostatic inkjet belong to drop-on-demand inkjet.

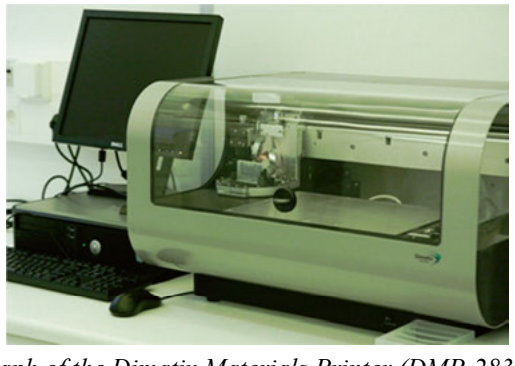

Figure 9. Photograph of the Dimatix Materials Printer (DMP-2831) used in this thesis work.

In this thesis, inkjet printing is carried out on a Dimatix Materials Printer (DMP-2831, Figure 9) with a piezo-based inkjet print cartridge (10 pl drop volume). Each single-use cartridge has 16 nozzles linearly arranged. Conductive ink is filled into a cartridge by a syringe. The substrates, including glass, PET, PDMS, silicon wafer and photo paper, are kept at 60 °C during printing.

The conductive inks were prepared by mixing graphene dispersion and reactive silver solution at different volume ratios. 2,3-butanediol was adopted to tune the viscosity that monitored by a viscosity meter. The reactive silver solution was prepared based on literature report, in which a modified Tollens' process was involved.[129] The modified Tollens' process exhibits some advantages in comparison with the typical Tollens' process. Silver acetate is used instead of silver nitrate for a more stable and nonexplosive silver precursor ink. Only carbon dioxide and water are the byproducts by using formic acid, avoiding residual reducing agent.[130] The modified Tollens' process involves the following reactions:

$$2\,CH_3COOAg + 2\,NH_4OH \xrightarrow{H_2O} Ag_2O + 2\,CH_3COONH_4 + H_2O \quad (3.4)$$

$$Ag_2O + 4\,NH_3 + 2\,CH_3COONH_4 + H_2O \xrightarrow{NH_3/H_2O} 2\,Ag(NH_3)_2CH_3CO_2 + 2\,NH_4OH \quad (3.5)$$

$$2\,Ag(NH_3)_2CH_3CO_2 + NH_4CO_2 \xrightarrow{\Delta} 2\,Ag + 5\,NH_3 + 2\,CH_3COOH + CO_2 + H_2O \quad (3.6)$$

$$2\,Ag(NH_3)_2CH_3CO_2 + NH_4CO_2 \longrightarrow Ag + AgCH_3CO_2 + 5\,NH_3 + 2\,CH_3COOH + CO_2 + H_2O \quad (3.7)$$

3.3 Electroless deposition

Electroless deposition is a non-galvanic plating method, which means no external current is required. It is an autocatalytic redox reaction, in which metal ions in solution are reduced to form a metal layer.[131] The plating process is carried out with a catalyst to initiate the reaction. High quality of site-selective immobilization of the catalyst results in a high spatial resolution of the electroless deposition. It has been used in practice for centuries since its coatings are continuous and uniform.

Compared to the electroplating, which requires strict experimental conditions, conductive substrates and power sources, electroless deposition is a much simpler process. The substrates could be conductor and insulator (like glass, plastic or ceramic) in the electroless deposition. It is a low-cost and low-temperature process.

Electroless deposition is employed in the fields of metallization of fabrics, polymers and yarns to achieve conducting materials for flexible and durable electronics, and attracts lots of interest in recent years. The adhesion between the deposited metal layer and the substrates is a big challenge.[132-133] Various ways have been used to improve the adhesion, such as employing polyelectrolyte brushes as the adhesion layers.[134] Deposition of different kinds of metals (such as copper, silver, nickel, gold, cobalt, palladium and iron) and their alloys has been achieved by this method and various reducing agents (for example, formaldehyde, hydrazine, ascorbic acid, hydrogen, polyhydroxy alcohols, and hypophosphite) have been reported.[135] The generic reac-

tion of electroless deposition of metal (M) by using a reducing agent (R^{m-}) can be expressed as:

$$M^{n+} + R^{m-} \rightarrow M + R^{n-m} \tag{3.8}$$

3.4 Characterization techniques

3.4.1 Characterization of electrical resistivity

Electrical resistivity is a measure of how strongly a material opposes the flow of electric current. It is represented by ρ and the unit is Ohm-meters (Ω·m) in International System of Units. It is defined as the ratio of the electric field inside a material to the electrical current density through it. The material with lower electrical resistivity more readily conducts a flow of electrical charge. Electrical conductivity is the reciprocal of electrical resistivity. It is represented by σ and the unit is Siemens per meter (S/m).

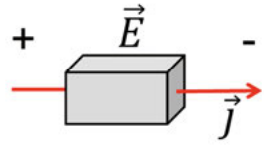

Figure 10. The illustration of electric field and current density in a material.

$$\rho = \frac{E}{J} \qquad \sigma = \frac{1}{\rho} = \frac{J}{E} \tag{3.9}$$

where E is the electric field in a material (in V/m) and J is current density through the material (in A/m^2).

The electrical resistance for a uniform material with known geometry can be measured in a direct way (Figure 11a) and electrical resistivity can be calculated by the following equation:

$$R = \rho \times \frac{L}{A} \quad \Rightarrow \quad \rho = R \times \frac{A}{L} \tag{3.10}$$

where R is measured resistance (in Ohm); L and A are the length (in m) and the cross-section area (in m^2) of the measured sample. The method is simple and straightforward, but the contact resistance is usually involved.

Two-point probe (Figure 11b) and four-point probe (Figure 11c) are commonly used to measure the resistance of thin films. In two-point probe measurement, it is difficult to accurately separate either contact resistance R_c between probes and sample surface or spreading resistance R_{sp} from the ma-

terial resistance of interest. Four-point probe method can avoid the influence from the wirings and contacts, which is a key advantage. One configuration is that the probes are arranged in-line with equal spacing (*s*), in which the two outer probes apply a constant current and the two inner probes measure the potential difference between them. With an ultrahigh internal resistance, almost no current flows through the sense loop. The typical probe radius ranges from 30 to 500 μm and probe spacing is in the range of 0.5-1.5 mm. In order to eliminate the size effect of finite geometry in four-point probe, the sample width should generally be forty times larger than probe spacing.[136] Sample thickness is one of the correction factors in the data processing.[137] Most of the samples measured in this thesis were performed using four-point probe.

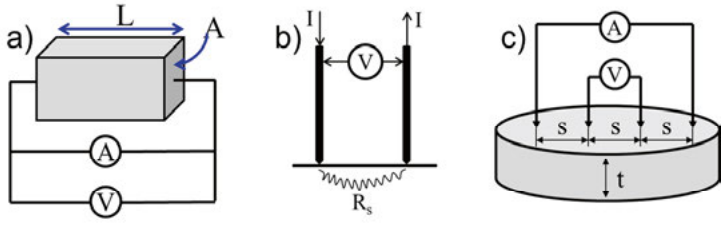

Figure 11. a) Direct measurement; b) two-point probe; c) four-point probe.

The graphene/Cu thin film in **Paper II** has a two-layer structure. The conductivity of the Cu layer can be extracted based on the known parameters: σ_{G}, t_{G}, σ_{Cu} and t_{Cu} for the graphene and Cu layer conductivity and thickness, respectively.

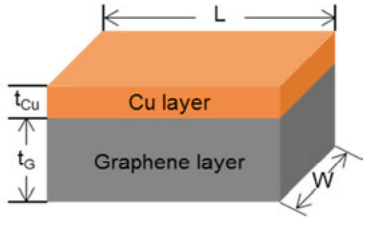

Further, *W* is the width (in m) of the thin film. The total resistance (*R*) of the graphene/Cu thin film is then given by:

$$R = \frac{R_G \times R_{Cu}}{R_G + R_{Cu}} \tag{3.11}$$

Therefore, the resistance of the Cu layer can be expressed by:

$$R_{Cu} = \frac{R \times R_G}{R_G - R} \tag{3.12}$$

and the conductivity of Cu layer can be calculated by following equation:

$$\sigma_{Cu} = \frac{1}{\rho_{Cu}} = \frac{L}{R_{Cu} \times W \times t_{Cu}} \quad (3.13)$$

The conductivity of Cu layer is calculated to be ~7×10^6 S/m, according to the known values in **Paper II** (σ_G = 110 S/m, t_G = 1.8 μm, $\sigma_{Total} = 7.9 \times 10^5$ S/m, t_{Cu} = 0.25 μm). Compared with conductivity of bulk Cu (5.96×10^7 S/m), the conductivity of Cu layer is one order of magnitude lower. The reason can be the presence of grain boundaries and impurity in the grown Cu layer.

3.4.2 Characterization of porosity and bulk conductivity of aerogel

Characterization of porosity of Cu/Cu_xO@rGO aerogel

The porosity (ϕ) of a porous material describes the fraction of void volume in the material, defined by:

$$\phi = \frac{V_V}{V_{Total}} \quad (3.14)$$

where V_V is the total volume (in m^3) of voids and V_{Total} is the bulk volume (in m^3) of the material.

The porosity can be calculated by the following form if the voids are filled up with air:

$$\phi = 1 - \frac{\rho}{\rho_{Bulk}} \quad (3.15)$$

where ρ is the apparent density of the material (in g/cm^3) and ρ_{Bulk} is the bulk density (in g/cm^3) that refers to the density of the compact solid material without void.

The bulk density of Cu/Cu_xO@rGO aerogel is mainly contributed by carbon and copper, which can be calculated through the following equation:

$$\rho_{Bulk} = \frac{m_{Total}}{m_C/\rho_C + m_{Cu}/\rho_{Cu}} \quad (3.16)$$

The density of carbon (ρ_C) and copper (ρ_{Cu}) are known as 2.26 g/cm^3 and 8.96 g/cm^3, respectively. The mass of carbon (m_C) and copper (m_{Cu}) are 72.15% and 27.85% of the total mass of Cu/Cu_xO@rGO aerogel according to the XPS characterization in **Paper IV**. Hence, the calculated bulk density is 2.86 g/cm^3 for the Cu/Cu_xO@rGO aerogel.

The apparent densities of Cu/Cu_xO@rGO aerogel are 0.065 g/cm^3 and 2.2 g/cm^3 prior to and after mechanical compression, using the bulk mass and volume for the calculation. Based on the calculated bulk density and apparent densities, the porosity of the aerogel is ~97.7% and ~23.1% prior to and after the mechanical compression, respectively.

Characterization of bulk conductivity of Cu/Cu_xO@rGO aerogel

It is known that the apparent conductivity of a porous material is sensitive to its porosity. Higher value of porosity results in lower apparent conductivity. According to the distribution of pores in the material, the relationships between the ratio of apparent conductivity/bulk conductivity (σ/σ_0) and porosity (ϕ) can be presented as equations (3.17)-(3.20) with different pore geometries.[138-139] All the pores are assumed to be homogeneously distributed in the material.

The relationship between σ/σ_0 and ϕ is:

$$\sigma/\sigma_0 = 1 - \phi \quad (3.17)$$

assuming the pores are cylindrical and parallel to the electric field,

$$\sigma/\sigma_0 = (1 - \phi)/(1 + \phi) \quad (3.18)$$

assuming the pores are cylindrical and perpendicular to the electric field,

$$\sigma/\sigma_0 = (1 - \phi)/(1 + 0.5\,\phi) \quad (3.19)$$

assuming the pores are spherical,

$$\sigma/\sigma_0 = (1 - \phi)^{3/2}/(1 + 0.5\,\phi) \quad (3.20)$$

assuming the pores are cubic, respectively. The relationships of equations (3.17)-(3.20) are visualized below:

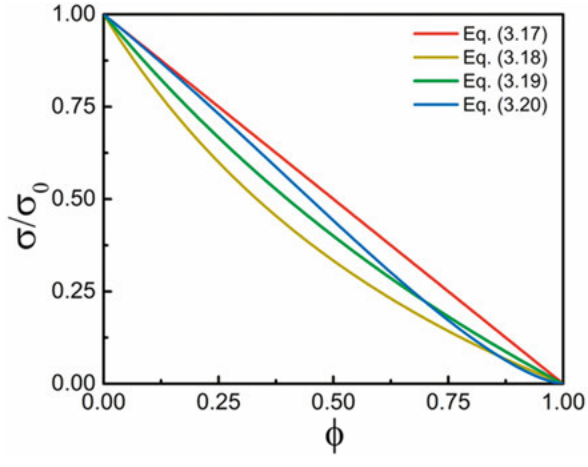

Figure 12. Relationships between σ/σ_0 and ϕ with different assumptions on the pore structure.

According to the literature,[138] equations (3.17)-(3.20) display large variation from the true relationship of σ/σ_0 *vs.* ϕ for $\phi > 0.55$. Therefore, it is valid to calculate the bulk conductivity of aerogel using the value of porosity

(23.1%) after mechanical compression. Based on equations (3.17)-(3.20), the calculated bulk conductivities are 559 S/m, 688 S/m, 624 S/m and 711 S/m using the known apparent conductivity (430 S/m) and porosity (23.1%) of the compressed aerogel, respectively. It is noted that the values of the bulk conductivity extracted from different models with different assumed geometries are at the same level. It is very likely that the bulk conductivity is mainly constrained by the interconnected rGO sheets as the copper nanoparticles are discretely attached on the surface of rGO.

3.4.3 Characterization of structural properties and composition

The morphology of the samples was investigated by both scanning electron microscope (SEM) and transmission electron microscopy (TEM). The SEM images in **Paper III** were carried out on a Merlin SEM (Zeiss, Germany) and the SEM images in the other papers were recorded using Zeiss 1530 scanning electron microscope (Carl Zeiss, Germany). The TEM imaging in **Paper II** and **Paper IV** was performed with Titan Themis 200 (FEI, USA) operated at 200 kV.

Raman spectroscopy is widely used in material analysis, especially in graphene research. It is a powerful tool to identify the number of layers and structural defects of graphene. Three distinct peaks (G, D and 2D peaks) can be observed from the Raman spectrum of graphene. The Raman spectra in all the papers were obtained on a Renishaw "inVia" Raman spectroscope (Renishaw, UK) with 532 nm laser and 20× lens.

Powder X-ray diffraction (XRD) is a non-destructive tool for phase investigation of a crystalline material. Siemens D5000 XRD (Siemens, Germany) used in **Paper I** aimed to observe the re-orientation of the individual graphene flakes. The presence of copper in **Paper II** was proved using a Bruker D8 Advance XRD Twin-Twin instrument (Bruker, Germany) with Cu-Kα radiation (λ = 1.5418 Å). The presence of rGO, copper and oxidized copper in **Paper IV** was explored by XRD using a Bruker D8 Advance Eco instrument (Bruker, Germany) with Cu-Kα radiation (λ = 1.5418 Å).

X-ray photoelectron spectroscopy (XPS) is a surface sensitive characterization technique to detect the chemical composition and respective valence states. The XPS spectra in **Paper III** were obtained by a PHI Quantum 2000 Scanning ESCA microprobe (Physical Electronics, USA). And XPS spectra in **Paper II** and **Paper IV** were achieved on a PHI Quantera II scanning XPS microprobe (Physical Electronics, USA).

4 Results and discussion

In this chapter, the main results of Paper I to Paper IV are summarized, including conductive graphene thin film, conductive graphene/Cu thin film, as well as conductive graphene/Ag and Cu/Cu_xO@rGO composites. All the conductive graphene-based materials mentioned here were fabricated by simple processes with low cost, low temperature and solution-phase production, demonstrating the promising future of conductive graphene-based materials in flexible electronics.

4.1 Conductive graphene thin film (Paper I)

In order to achieve flexible interconnects by a solution-phase method, deposition of the conductive materials onto substrates is a necessary step. As mentioned previously, graphene has been a promising flexible conductive material due to its unique electronic, mechanical and thermal properties.[98, 101-102] However, in most previous literature reports, graphene thin films deposited from solution exhibit inferior electrical conductivity due to poor control over the microstructure in the film and poor physical contact among the individual graphene flakes. Individual graphene flakes orient randomly when a droplet lands on a substrate and dries out, which leads to a film of weakly interconnected graphene flakes. The film thus exhibits porous feature with low density which usually leads to relatively poor electrical conductivity. Hence, how to effectively remedy the defective aspects of graphene thin films directly deposited from dispersion and therefore to improve the conductivity of the thin films is still a largely unsolved challenge. For this purpose, it is necessary to densify as-deposited graphene films and align the graphene flakes in the films. In this way, inter-flake contact area can be maximized for a reduction of the contact resistance.

Here, a post-deposition treatment method was used to re-orient individual graphene flakes in graphene films. This method is present in Figure 13. Drops of aqueous graphene dispersion with cellulose stabilizer ((hydroxypropyl)methyl cellulose (HMC)) were casted on a glass substrate and subsequently baked on a hot plate (200 °C or 300 °C). The resultant graphene films exhibit poor uniformity and rough surface. The post-deposition treatment step involves soaking of the as-prepared graphene films in DI water followed by a heat treatment (300 °C). As a result, the graphene thin films

were significantly densified and smoothened. A possible mechanism is that the remaining HMC is water soluble and water can disconnect the individual graphene flakes from the weakly interconnected porous frame. Graphene flakes settle down under gravity force and trend to orient horizontally and attach to each other in a face to face manner. Meanwhile, during the subsequent heating, the water tends to flow horizontally as the graphene flakes provide capillary-like channels, which drives the graphene flakes in the thin films to re-orient horizontally.

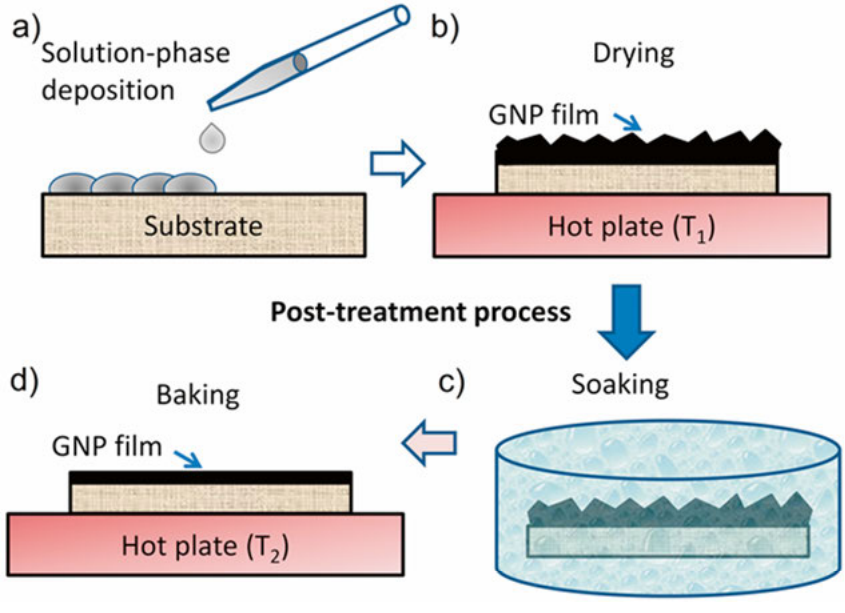

Figure 13. Schematic illustration of the two-step deposition procedure from aqueous dispersion. Reprinted with permission from [140]. Copyright (2018) Elsevier.

The comparison of SEM images (Figure 14a-b) showed that the graphene flakes underwent re-organization during the post-treatment, i.e., the soaking and drying step. The flakes became more horizontally oriented and the film surface was flattened. XRD (Figure 14c) further demonstrated the horizontal orientation of graphene flakes after the post-treatment. And probe profile meter measurement (Figure 14d) showed the decreased thickness and more uniform thin film. The resultant films exhibited increased electrical conductivity, changing from 50-100 S/m for the prior re-organized films to 1000-3000 S/m after. This method provides a simple way to densify, smoothen and homogenize graphene thin films, and is universally applicable to solution-phase film deposition of any other 2D materials.

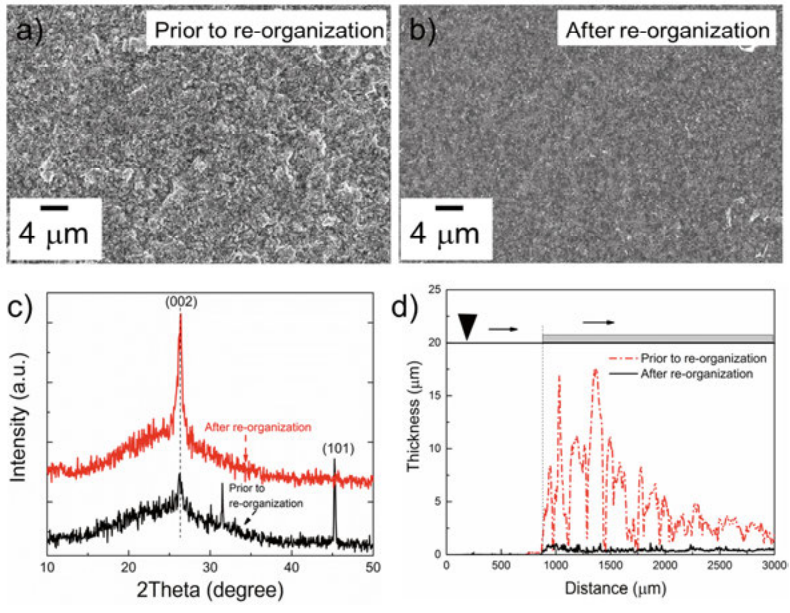

Figure 14. a-b) Selected SEM images of graphene thin films prior and after re-organization; c) XRD of graphene thin films prior and after re-organization; d) probe profile measurement of graphene thin films prior (dashed line) and after (solid line) re-organization. Adapted with permission from [140]. Copyright (2018) Elsevier.

Summary

A simple post-deposition treatment method has been developed to re-organize the individual graphene flakes in the films and thus dramatically densify the films. An enhanced electrical conductivity at the level of ~3 × 10^3 S/m is obtained as a result. However, the value is still insufficient for the interconnect application. To solve the problem, a synergic effect can be employed to enhance the performance of conductivity. Hybrid graphene/metal thin film and graphene/metal composites likely provide solutions to the enhancement in the conductivity, which will be discussed in the following parts (Paper II to Paper IV).

4.2 Conductive graphene/Cu thin film (Paper II)

Copper metallization plays an important role in the fabrication of printed circuit boards, chip interconnects, magnetic storage devices and many other applications in microelectronics industry. Copper metallization can be achieved by different strategies, including electrochemical plating, electroless deposition, physical vapor deposition (PVD), and CVD.[134, 141-142] Compared to the vapor deposition methods, electroless deposition exhibits the

advantage of low cost and low temperature processing. It is also suitable for any substrates including the insulating ones (such as polymer substrates), which is superior to electrochemical plating as it requires a conductive surface. The deposition process is accomplished in the presence of a catalyst which initiates the reaction. Hence, site-selective immobilization of the catalyst allows for self-aligning of the deposited metal layer.

Since quaternary ammonium groups (QA^+) show good affinity to the $PdCl_4^{2-}$ species (a catalyst for electroless deposition of copper),[134] PyB-TBA is synthesized and utilized to immobilize the catalyst. It is assumed that PyB-TBA could act as both molecular wedge to expand the inter-layer distance at the edge of graphite and as stabilizer of graphene dispersion by forming π-π and cation-π interactions with the fresh graphene flakes surface. A conductive graphene/Cu thin film is expected to be fabricated by exfoliation of pristine few-layer graphene flakes and subsequent site-selective formation of Cu.

The graphene dispersion was produced by shear exfoliation in the presence of PyB-TBA in aqueous solution. A shadow mask was used to define the pattern of graphene thin film deposition (Figure 15a-c). And the procedure used for site-selective and self-aligned electroless deposition of Cu on the graphene films on PET substrate is shown in Figure 15d-e. After electroless deposition of Cu, the thin films were washed with DI water several times, dried by blowing with nitrogen gun and subsequently kept on a hot plate at 40 °C. The redox reaction of the electroless deposition of copper is as following:

$$2HCHO + Cu^{2+} + 4OH^- \rightarrow 2HCOO^- + Cu^0 + H_2 + 2H_2O \qquad (4.1)$$

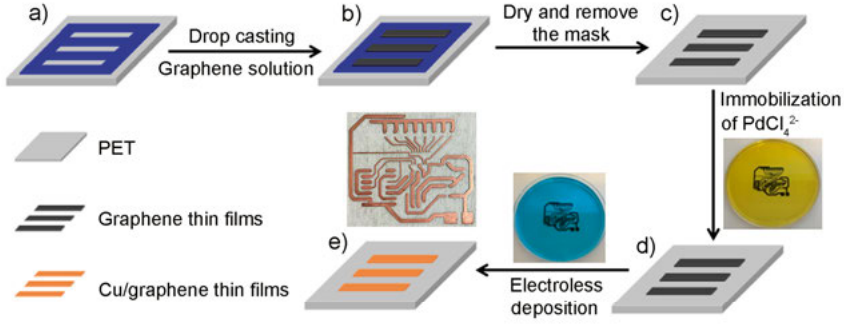

Figure 15. Schematic illustration of the procedure used for site-selective and self-aligned electroless deposition of Cu on the graphene films on PET substrate, where the real pattern is represented by three lines in the sketch. a-c) Formation of patterned graphene thin film on PET substrate; d-e) eletroless deposition of Cu. Reprinted with permission from [143]. Copyright (2019) American Chemical Society.

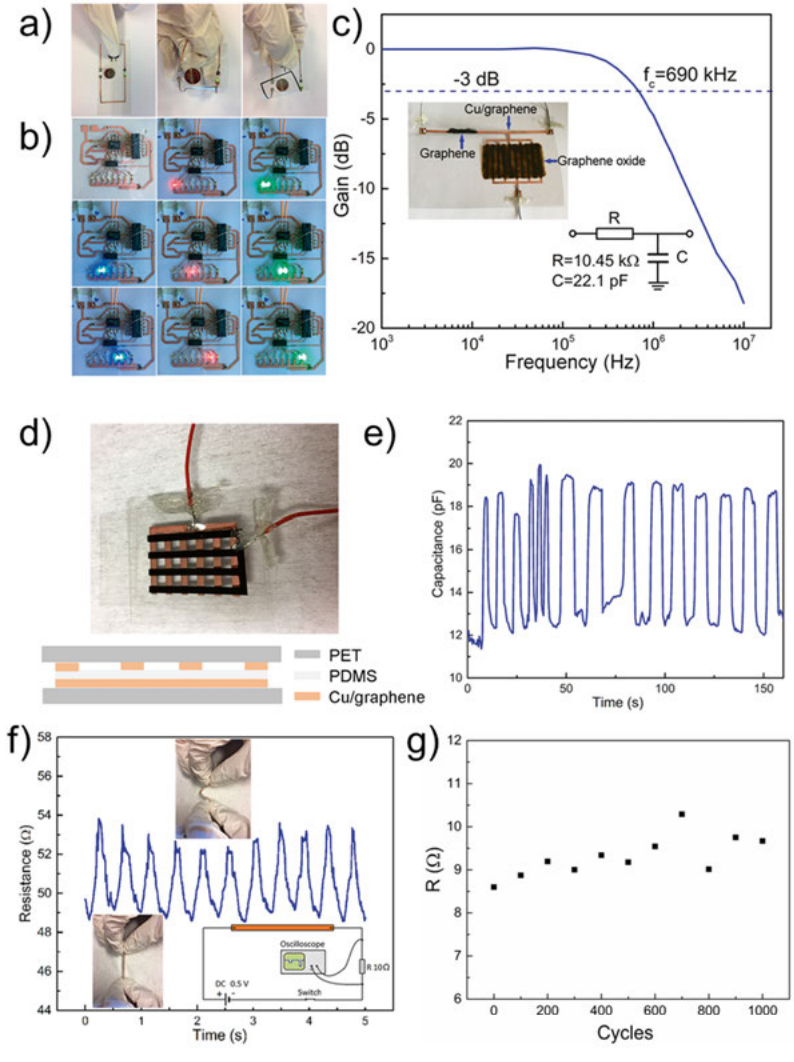

Figure 16. a) Photographs of simple electronic circuit; b) photographs of 8-LED sequentially illuminated circuit integrated with eight LEDs, 555 Timer, D-triggers, and 3-8 decoder (give time in each photo); c) performance of the low frequency filter (the insert images are the photographs of the filter and the circuit diagram); d) photograph and schematic illustration of a sandwich structural capacitor; e) capacitance vs. pressing/releasing cycles; f) relative resistances of graphene/Cu film vs. bending cycles in the bending test (the insert images are the circuit diagram of the bending tests and photographs of the released and compressed sample); g) the change in resistance of the graphene/Cu belt (5 mm × 30 mm) upon repeated bending cycles. Adapted with permission from [143]. Copyright (2019) American Chemical Society.

Use PyB-TBA as an exfoliation enhancer, few-layer graphene flakes populated with 2 to 4 layers have been achieved in water using a shear-mixing process. PyB-TBA also works as a dispersion stabilizer for the exfoliated

graphene flakes. An as-deposited graphene thin film containing PyB-TBA has a conductivity of ~110 S/m after being dried at 90 °C as opposed to that a similar film but with polymer stabilizer (e.g., HMC) treated at the same temperature behaves non-conductive. This result is of great interest as annealing at 90 °C is compatible well with most temperature-sensitive substrates. The subsequent electroless plated Cu of ~0.25 μm thickness on top of graphene film at room temperature leads to an apparent conductivity to ~7.9×10^5 S/m. The superimposed Cu layer alone exhibits conductivity of ~7.8×10^6 S/m, which is only seven times lower than that of bulk Cu (~5.8×10^7 S/m).[144] In addition, the Cu plating is self-aligned to the pre-defined graphene patterns due to the immobilization of catalyst by PyB-TBA.

Because of the high conductivity and self-alignment production of the graphene/Cu, several circuits made on plastic foils, including low frequency filter and sandwich structural capacitor as shown in Figure 16, were demonstrated. The graphene/Cu films are robust upon mechanical bending. A 5 mm × 30 mm graphene/Cu belt was used to do the cyclic tests and its resistance was changed by only 5% after the sample was repeatedly bended for 1000 cycles.

Summary

Efficient shear-mixing exfoliation of pristine few-layer graphene flakes from graphite in aqueous solution and subsequent site-selective formation of highly conductive graphene/Cu films have been obtained by using the water-soluble PyB-TBA. The facile solution-phase, low temperature processing and self-alignment procedure to achieve graphene/Cu film with high apparent conductivity may facilitate the fabrication of electronic circuits using graphene/Cu films as flexible interconnects on plastic foils. However, one drawback of this method lies in its requirement of two steps, i.e., graphene film deposition followed by electroless Cu plating. From manufacturability and cost-effectivity points of view, one-step processes can be superior to two-step ones. One approach towards one-step process for patterned interconnects is based on printed composites with graphene flakes and metal which will be presented in the following work (Paper III). The composites are expected to enhance the specific strength, electrical and thermal conductivity. The presence of metal nanoparticles decreases the contact resistance of graphene junctions and simultaneously graphene builds effective electrical pathways between aggregated metal nanoparticles to reduce the negative influence of voids. In addition, the presence of graphene can decrease the amounts of metal, leading to a cost effective manufacture.

4.3 Conductive graphene/metal composites

4.3.1 Conductive graphene/Ag composite (Paper III)

In order to achieve low-cost and large area electronic devices and effectively utilize the unconventional flexible substrates (such as plastic foils, polymeric foils, textile and paper), the employment of printing technology is a promising solution.[145-146] Compared to the conventional electronics, printed electronics possess the advantages of large areas, simple fabrication, flexible, as well as low fabrication costs. Printed conductors, such as interconnects in electronic circuit and electrodes in energy storage/conversion devices, are key components of printed electronics devices.

Pure metal nanoparticles, conducting polymers and graphene are commonly used in printed conductors. However, some critical issues cannot be ignored for the development of printed conductors. The low electrical conductivity of conducting polymers,[90] high sintering temperatures and high cost of silver,[147-148] oxidation of copper in ambient atmosphere,[81] limited electrical conductivity of graphene thin film produced from solution phase as presented above have to be taken into account. To solve the aforementioned problems, graphene/metal composites utilizing a synergic effect have emerged. Graphene/Ag composite is the most explored kind of graphene/metal composites due to the fact that Ag is more cost effective in comparison with Pd or Au and more stable than Cu since Cu in nanostructure is easy to be oxidized in ambient atmosphere. Graphene/Ag composite can possess a good combination of electrical conductivity, mechanical strength, reliability and cost efficiency, which render it suitable for interconnect application.

Here, a facile method is presented to prepare conductive composite inks by mixing pristine few-layer graphene aqueous dispersion and reactive silver aqueous solution at different volume ratios. Graphene dispersion was produced by shear-mixing exfoliation and HMC was introduced as stabilizer in aqueous solution. The reactive silver solution was prepared based on the literature, in which a modified Tollens' process was involved.[129] The viscosity of the hybrid mixture was adjusted using 2,3-butanediol. Graphene/Ag films were achieved by inkjet printing of the formulated inks. After inkjet printing, the samples were annealed at 100 °C for 20 min on a hotplate. What should be mentioned here is that the conductive graphene/Ag hybrid ink can be deposited with a good patterning quality on a variety of untreated substrates (Figure 17), including glass, PET, PDMS, silicon wafer, and photo paper as compared with the aqueous silver ink without graphene. An interesting result is found on the photo paper substrate, which is that the printed films only appear on the front side of the photo paper. The silver ink without graphene permeates to the rear side of the photo paper, which is unwanted in

applications. The superior printability of the composite ink can make it applied well to paper electronic devices.

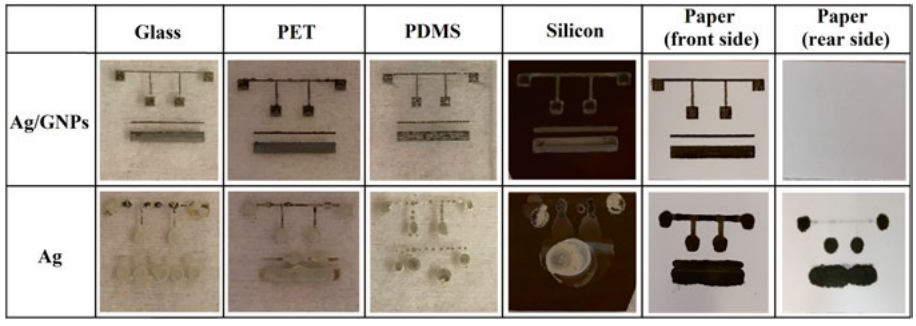

Figure 17. Photographs of the printed graphene/Ag composite films (Ag/GNPs, upper) and silver (Ag, lower) on various substrates. Reprinted with permission from [149]. Copyright (2018) IOP Publishing.

The printed graphene/Ag composite thin films show different microstructure features at different nominal volume ratio of silver solution and graphene dispersion. The 1:1 volume ratio shows that the graphene flakes are embedded in a silver matrix and the silver matrix is composed of interconnected silver particles with size ranging from 50 nm to 200 nm (Figure 18a-b). The 1:2 volume ratio exhibits that all the graphene flakes are well-covered with a layer of silver and the silver-coated graphene flakes stand up and are interconnected forming a porous network (Figure 18c-d).

The printed graphene/Ag composite thin films exhibit electrical conductivity beyond 10^6 S/m by annealing at 100 °C for 20 min, which can be attributed to the synergic effect between graphene and Ag. The presence of Ag nanoparticles on the surface of graphene sheets decreases the contact resistance of graphene junctions. Simultaneously, Ag and graphene build effective electrical pathways, separately. The formation of the former most likely is responsible for the achieved high apparent electrical conductivity. A simple electronic circuit on PET is demonstrated (Figure 18e), in which a button battery, light-emitting diode (LED) and switch were connected to the printed composite tracks. The brightness of the LED remained unchanged when the printed electronic circuit was folded in any shape, proving the mechanical flexibility and robustness of the composites.

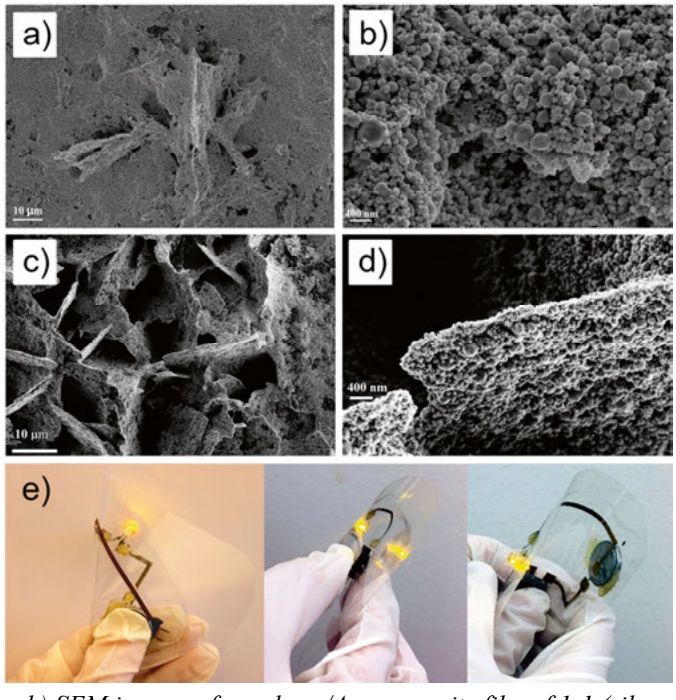

Figure 18. a-b) SEM images of graphene/Ag composite film of 1:1 (silver solution to graphene dispersion) nominal volume ratio; c-d) SEM images of graphene/Ag composite film of 1:2 (silver solution to graphene dispersion) nominal volume ratio; e) photographs of an inkjet-printed electronic circuit on PET substrate. Adapted with permission from [149]. Copyright (2018) IOP Publishing.

Summary

Highly conductive and morphology-tunable graphene/Ag composite films on various substrates have been readily obtained by inkjet printing. The printed graphene/Ag composite films show high electrical conductivity beyond 10^6 S/m after annealing at 100 °C for 20 min. The availability of graphene/Ag composite films paves the way to the metallization in a variety of printed devices, such as interconnects in printed circuits and electrodes in energy storage/conversion devices. Even though the highly conductive composite obtained by mixing graphene flakes and silver ions in dispersion has been developed, the development of a more cost-effective composite is still necessary. Silver is expected to be replaced by some cheaper metal. Copper is considered as a promising candidate due to its earth abundance. It is much cheaper than silver and has conductivity close to that of silver. GO has advantages of low cost and high dispersibility in water. It is therefore worthwhile to explore the combination of copper and GO for hybrid ink and composite which will be presented below (Paper IV).

4.3.2 Conductive Cu/Cu_xO@rGO composite (Paper IV)

Due to its high dispersibility in aqueous media and abundant oxygen-containing groups, GO is a promising precursor to fabricate graphene/metal composite although reduction in GO has to be considered. An attempt to prepare hybrid ink with aqueous graphene oxide solution and copper-contained Fehling's solution unexpectedly resulted in a macro-assembling of highly conductive 3D rGO/copper hybrid (Cu/Cu_xO@rGO) hydrogel at room temperature. Aerogel is obtained *via* freeze-drying of the hydrogel. Since aerogels possess the unique properties of interconnected 3D porous structure with high specific surface area, extremely low density and good mechanical property, they can be applied in the fields of catalysis, energy storage/conversion, environmental remediation and gas sensing.[150-155]

The preparation of hydrogel starts from GO water dispersion (0.4 wt%, 6 mL) mixed uniformly with 0.5 mL of $(NH_4)_2PdCl_4$ aqueous solution (5 mM) and 12 mL of 1:1 mixture of freshly Fehling's reagent solution (0.012 g/mL NaOH, 0.029 g/mL potassium sodium tartrate tetrahydrate and 0.013 g/mL $CuSO_4 \cdot 5H_2O$) and formaldehyde solution (9.5 μL/mL). The mixture was filled in a cylindrical vial and kept overnight at room temperature. During the formation of Cu/Cu_xO@rGO hydrogel, GO was reduced to rGO and the resulting rGO was self-assembled into 3D hydrogel. At the same time, Cu_xO nanoparticles attached on the rGO sheets together with the Cu nanoparticles. A subsequent freeze-drying of the hydrogel leads to aerogel. The aerogel of rGO network decorated with Cu/Cu_xO nanoparticles shows apparent electrical conductivity of ~33 S/m and ~430 S/m prior to and post mechanically compression.

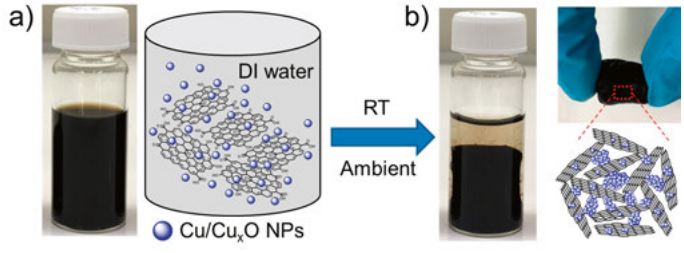

Figure 19. Illustration of the formation of Cu/Cu_xO@rGO hydrogel. Reprinted with permission from [157].Copyright (2019) Elsevier.

Since the conductive Cu/Cu_xO@rGO aerogel possesses porous structure and Cu/Cu_xO nanoparticles are randomly attached on the surface of rGO sheets, it is expected to be useful for energy storage. The electrochemical measurements in Figure 20d reveal the battery-type of characteristic. Galvanostatic charge-discharge (GCD) measurements (Figure 20a) show that the as-prepared Cu/Cu_xO@rGO aerogel electrode performs a specific capacity of the value of ~453 mAh g^{-1} at a current density of 1 A/g. And the capacity still retained 41% along with the current density increasing to 50 A/g (Figure

20b), revealing the good rate capability. Long-term charge-discharge process in three-electrode cell was performed at the current density of 5 A/g to investigate the cycling stability of Cu/Cu_xO@rGO aerogel (Figure 20c). The Cu/Cu_xO@rGO aerogel initially exhibits a specific capacity of ~339 mAh g^{-1} and retained 38% (129 mAh g^{-1}) after 500 cycles. The possible reasons for the decrease of specific capacity during the long-term charge-discharge process include long-time immersion of Cu/Cu_xO@rGO aerogel electrode in the abundant electrolyte could result in detaching of the Cu/Cu_xO@rGO aerogel film from the underlying graphite paper and the dissolving of the soluble $Cu(OH)_4^{2-}$ species.

The gravimetric capacity (C_G) of Cu/Cu_xO@rGO aerogel was calculated from GCD curves using the following equation:

$$C_G = \frac{I \times \Delta t}{m} \tag{4.2}$$

where I is the current (in mA), Δt is the discharge time (in s), m is the mass of Cu/Cu_xO@rGO aerogel electrode (in g).

The volumetric capacity (C_V) of Cu/Cu_xO@rGO aerogel was calculated from GCD curves using the following equation:

$$C_V = \frac{I \times \Delta t}{V} \tag{4.3}$$

where V is the volume of Cu/Cu_xO@rGO aerogel electrode (in cm^3).

The possible reaction processes in the cyclic voltammetry (CV) measurement are indicated in the following equations.[156] The oxidation peak at −0.32 V (*vs.* Hg/HgO) at scan rate of 10 mV/s corresponds to reaction (4.4) with the formation of Cu_2O, while the one at 0.05 V (*vs.* Hg/HgO) is associated with reactions (4.5-4.8) yielding different Cu^{2+} complexes ($Cu(OH)_4^{2-}$, $Cu(OH)_2$ and CuO). On the oxidation scan, the Cu_2O is hence first formed, followed by a further oxidation to Cu^{2+} as the potential is increased further.

$$2\ Cu + 2\ OH^- \rightarrow Cu_2O + H_2O + 2\ e^- \tag{4.4}$$

$$Cu_2O + H_2O + 6\ OH^- \rightarrow 2\ Cu(OH)_4^{2-} + 2\ e^- \tag{4.5}$$

$$Cu_2O + H_2O + 2\ OH^- \rightarrow 2\ Cu(OH)_2 + 2\ e^- \tag{4.6}$$

$$Cu + 4\ OH^- \rightarrow Cu(OH)_4^{2-} + 2\ e^- \tag{4.7}$$

$$Cu + 2\ OH^- \rightarrow CuO + H_2O + 2\ e^- \tag{4.8}$$

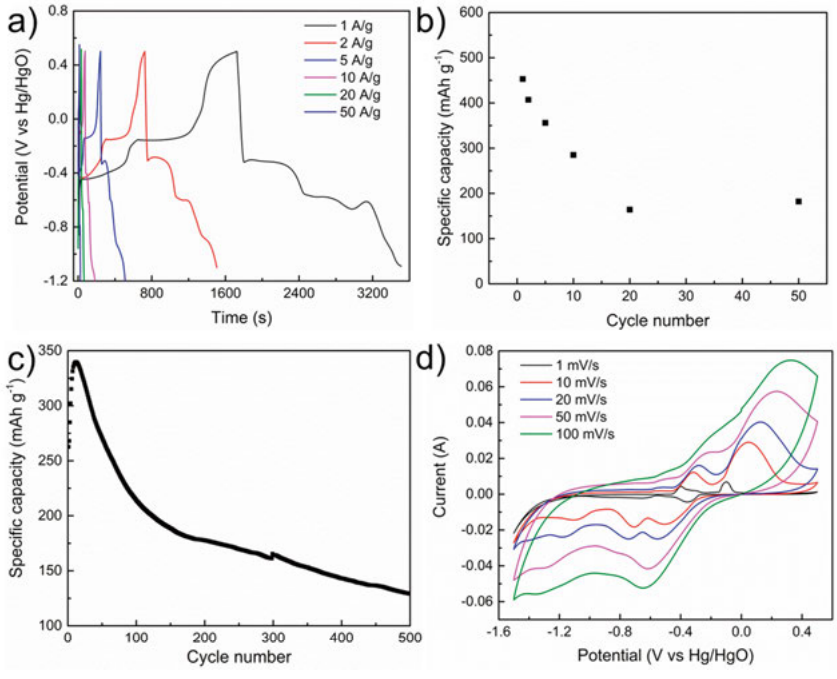

Figure 20. a) Galvanostatic charge-discharge curves of the Cu/Cu$_x$O@rGO hydrogel electrode; b) variation in the specific capacity of the Cu/Cu$_x$O@rGO hydrogel as a function of current density; c) cycling stability of the Cu/Cu$_x$O@rGO hydrogel during long-term charge-discharge process at a current density of 5 A/g; d) CV curves of the Cu/Cu$_x$O@rGO hydrogel at different scan rates. The voltammograms were recorded starting with an oxidation from the OCV to 0.5 V followed by a reductive scan to −1.5 V (vs. Hg/HgO). Adapted with permission from [157]. Copyright (2019) Elsevier.

Summary

A simple synthesis of Cu/Cu$_x$O@rGO hydrogel with rGO network decorated with Cu/Cu$_x$O NPs under ambient condition is presented. A subsequent freeze-drying of the hydrogel leads to aerogel, which exhibits an apparent electrical conductivity of ~430 S/m and could deliver a specific capacity of ~453 mAh g^{-1} at a current density of 1 A/g after being mechanically compressed. The high conductivity and good performance in electrochemical measurements, as well as the facile synthesis method of the Cu/Cu$_x$O@rGO aerogel exhibit potential application in the area of energy storage.

5 Conclusions and future perspective

This thesis has spanned from graphene thin films with inferior conductivity to highly conductive graphene/metal hybrid materials, which were fabricated by simple procedures with low cost, low temperature and solution-phase production. The developed materials exhibit promises for flexible electronics and energy storage applications. It was found that graphene flakes in an as-deposited film from dispersion can be efficiently re-oriented by a simple post-deposition treatment leading to a significant conductivity enhancement. The self-aligned electroless deposition creates two-layer graphene/Cu thin film of rather high electrical conductivity which allow us to readily fabricate various electronic circuits including an 8-LED sequentially illuminated circuit, low frequency filter and sandwich structural capacitor on plastic foils. Alternatively, graphene/Ag composites can be achieved by inkjet printing showing electrical conductivity higher than 10^6 S/m after annealing temperature only at 100 °C. When using graphene oxide instead of pristine graphene mixed with copper-containing solution, a highly conductive hydrogel with rGO and copper components (Cu/Cu_xO@rGO) was achieved with a high potential for application in energy storage. The bottlenecks for copper oxide only used as electrode material are their very low electrical conductivity and capacity losses upon charging-discharging processes. More efforts are underway to develop and additively fabricate flexible electronics of outstanding performances combined with advantages in low cost, energy efficiency, and environmental friendliness.

One of the crucial aspects towards the advancement of flexible electronics is the development of inexpensive conductive materials with enhanced performance and reliability. Hybrid materials deserve more attention due to their inherited advantages of all the components by synergic effects. In addition, utilization of solution-phase deposition technologies in production of electronic devices is necessary. The conductive materials should be compatible to the roll-to-roll process to increase product output and reduce production costs. Based on the current materials and techniques, further material development is expected for the additive manufacturing of 3D flexible electronics.

Sammanfattning på svenska

Avsikten med detta avhandlingsarbete var att, med flexibel elektronik i åtanke, utveckla högledande kompositmaterial baserade på grafenflagor, bestående av ett fåtal atomlager vardera, deponerade från vattenlösning och vidare processade vid låga temperaturer. Arbetet har motiverats av efterfrågan på nya elektriskt ledande material, med högre prestanda än de idag vanligt förekommande kompositmaterial innehålles nanopartiklar av silver eller koppar, och som kan mönstras till elektriska ledare över stora ytor via tryckning på flexibla substrat. I jämförelse med vakuumbaserade fabrikationsalternativ uppvisar deponering från dispersionslösning fördelar så som kostnadseffektivitet samt möjlighet till beläggning över stora ytor.

Grafen valdes som funktionell komponent vid beredningen av nya ledande kompositmaterial p.g.a. dess stora ytarea, kemiska inerthet samt utmärkta mekaniska, optiska, elektroniska och elektriska egenskaper. Emellertid uppvisar grafenfragmenten i tunna filmer deponerade från dispersioner normalt sett en slumpmässig orientering och låg packningsgrad, vilket påverkar filmens elektriska ledningsförmåga negativt. Ett resultat av avhandlingsarbetet är en enkel post-deponeringsbehandling för att orientera de individuella grafenflagorna och följaktligen dramatiskt höjer filmens densitet. Detta resulterar i en substantiell förbättring av den elektriska ledningsförmågan.

Tryckta filmer med innehåll av omodifierad grafen är i regel inte ledande utan en högtemperaturbehandlig, p.g.a. närvaron av polymera stabiliseringsmedel. Vid användning av lågmolekylära pyrene-derivat, t.ex. 1-pyrenebutyric acid tetrabutylammonium salt (PyB-TBA), kan effektiv exfoliering av grafen åstadkommas och ett grafenbläck med elektrisk konduktivitet om 100 S/m beredas, efter värmebehandling vid 100 °C. Därutöver möjliggör användningen av PyB-TBA en läges-selektiv, självlinjerad och elektrodfri deponering av koppar vid rumstemperatur. En sådan procedur resulterar i en distinkt tvålagersstruktur med en elektrisk konduktivitet om $\sim 7.9 \times 10^5$ S/m. Implementeringen av olika typer av elektroniska kretsar och komponenter har demonstrerats t.ex. kretsar innehållandes 8 sekventiellt tända LEDs, lågfrekvensfilter samt tunnfilmskondensatorer konstruerade av Cu/grafen på plastfolie.

Grafenfilmer, deponerade från vätskefas, har en elektrisk ledningsförmåga i storleksordningen 10^2 till 10^4 S/m, efter att ha värmebehandlats vid en temperatur om 300 °C eller högre, vilket inte är tillräckligt för att tjäna

som ledare för sammankoppling av komponenter. Bristfällig mönsteråtergivning kan erhållas för vissa typer av substrat vid användning av vattenbaserade grafenbläck i kombination med bläckstråleskrivare, med exempelvis diskontinuiteter i tilltänkt sammanhängande objekt. För att lösa dessa problem utnyttjades en synergistisk effekt som uppnås via blandning av grafenflagor med silverjoner och vilken möjliggör kompositmaterial med hög elektrisk ledningsförmåga och förbättrade mönstringsegenskaper. Detta resulterade i bulkkonduktivitet > 10^6 S/m efter en värmebehandling vid endast 100 °C, vilket är förenligt med temperaturkänsliga polymer-, gummi- och papperssubstrat.

Ett försök att tillbereda ett hybridbläck med en vattenlösning av grafenoxid samt kopparinnehållande Fehlings-lösning, resulterade oväntat i makroorganiseringen av ett högledande tredimensionellt (3D) grafenkopparhybrid- (Cu/Cu_xO@rGO) hydrogel vid rumstemperatur. En efterföljande frystorkning av hydrogelen resulterade i erhållandet av en aerogel. Aerogelen bestående av nätverk av reducerad grafenoxid (rGO) och dekorerad med Cu/Cu_xO-nanopartiklar, uppvisar konduktivitet om ~33 S/m. Elektrokemiska mätningar visar att Cu/Cu_xO@rGO-aerogelen har en specifik kapacitet om ~453 mAh g^{-1} vid en strömdensitet på 1 A/g och ~184 mAh g^{-1} vid 50 A/g i en 3M KOH(aq)-elektrolyt. Den goda ledningsförmågan och prestandan i elektrokemiska mätningar indikerar en stor potential för applikationer av Cu/Cu_xO@rGO-aerogel inom energilagring.

Sammanfattningsvis presenteras i denna avhandling vätskebaserade processcheman för implementering av elektriskt ledande grafenbaserade material i flexibel elektronik. De redovisade angreppssätten kan bana väg för utvecklingen av flexibel elektronik med enastående prestanda i kombination med egenskaper såsom låg kostnad, energieffektivitet och miljövänlighet.

Acknowledgement

I still remember the first day when I came to Uppsala. It feels like yesterday though four years have passed. Now I am going to finish my PhD study in Uppsala University. Thinking back to my life in the last four years, too many names come to my mind and too many thanks I want to say. It is a great honor to be here working with the wonderful colleagues and meeting those lovely friends. I would like to show my most sincere gratitude to all of you.

I would like to thank my supervisors *Zhi-Bin Zhang* and *Shi-Li Zhang* for giving me the opportunity to pursue my PhD in Uppsala University and for your help with the project discussions and paper revisions.

I would also like to thank my co-authors, *Chenyu Wen*, *Shuangshuang Zeng*, *Man Song*, *Malkolm Hinnemo* and *RuiJun Pan*, without whom I could not finish my project so successfully. Thanks to the MSL staff, with the help of whom I learned a lot in the cleanroom. Thanks to *Carl Hägglund* for the revision of the thesis, *Björn Landeke-Wilsmark* for the help of Swedish summary, *Lars Riekehr* for the assistance of TEM measurements, *Jonatan Bagge* for the IT support, *Jörgen Olsson* and *Ingrid Ringård* for the generous help.

Sincere thanks to *Ping Yan*, *Ao Gao*, and *Xingxing Xu* to be my room-mates, I have spent so many precious time with you. Thank you *Rui Sun* for being my close friend, we have had innumerable discussions about research and life, we have spent countless hours to be together for travelling, shopping and exercising. Thank you *Xi Chen* for sharing the delicious food and creating great time with me. *Qiuhong Wang*, thanks for being my nice neighbour and friend. *Si Chen* & *Ruixiang Xu*, thank you for inviting me to your home for dinner so many times and teaching me and Dong skiing. *Ngan Pham* is very much thanked for the warm talks. Thanks to *Qitao Hu* for many kind help. Thanks to all the colleagues and Chinese friends in Ångström.

I am also indebted to my supervisors *Biao W*u & *Xiao-Juan Yang* in Northwest University. You taught me so much about the attitude of doing research in the very beginning.

CSC is acknowledged for the financial support of my PhD study.

My deepest gratitude goes to my family! 谢谢亲爱的爸爸妈妈，是你们无条件的爱与支持，坚定了我前进的信念。谢谢亲爱的外公外婆，养育之恩，无以回报。谢谢栋的出现和陪伴，你的包容和宠爱给了我莫大的幸福，谢谢有你陪我共尝悲喜，给我依靠的肩膀。

References

1. Bao, Z.; Chen, X. Flexible and stretchable devices. *Adv.Mater.* **2016**, *28*, 4177-4179.
2. Han, S.-T.; Peng, H.; Sun, Q.; Venkatesh, S.; Chung, K.-S.; Lau, S. C.; Zhou, Y.; Roy, V. A. L. An overview of the development of flexible sensors. *Adv.Mater.* **2017**, *29*, 1700375.
3. Wang, J.-L.; Hassan, M.; Liu, J.-W.; Yu, S.-H. Nanowire assemblies for flexible electronic devices: recent advances and perspectives. *Adv.Mater.* **2018**, *0*, 1803430.
4. Gao, M.; Li, L.; Song, Y. Inkjet printing wearable electronic devices. *J. Mater. Chem. C* **2017**, *5*, 2971-2993.
5. Liu, Y.; He, K.; Chen, G.; Leow, W. R.; Chen, X. Nature-inspired structural materials for flexible electronic devices. *Chem. Rev.* **2017**, *117*, 12893-12941.
6. Nathan, A.; Ahnood, A.; Cole, M. T.; Lee, S.; Suzuki, Y.; Hiralal, P.; Bonaccorso, F.; Hasan, T.; Garcia-Gancedo, L.; Dyadyusha, A.; Haque, S.; Andrew, P.; Hofmann, S.; Moultrie, J.; Chu, D.; Flewitt, A. J.; Ferrari, A. C.; Kelly, M. J.; Robertson, J.; Amaratunga, G. A. J.; Milne, W. I. Flexible electronics: the next ubiquitous platform. *Proc. IEEE* **2012**, *100*, 1486-1517.
7. Cruz, S. M. F.; Rocha, L. A.; Viana, J. C., Printing technologies on flexible substrates for printed electronics. *Flexible Electronics*, IntechOpen **2018**.
8. Aleeva, Y.; Pignataro, B. Recent advances in upscalable wet methods and ink formulations for printed electronics. *J. Mater. Chem. C* **2014**, *2*, 6436-6453.
9. Li, D.; Lai, W.-Y.; Zhang, Y.-Z.; Huang, W. Printable transparent conductive films for flexible electronics. *Adv.Mater.* **2018**, *30*, 1704738.
10. Abbel, R.; Galagan, Y.; Groen, P. Roll-to-roll fabrication of solution processed electronics. *Adv. Eng. Mater.* **2018**, 1701190.
11. Wong, W. S.; Salleo, A., Flexible electronics: materials and applications. *Springer Science & Business Media* **2009**.
12. Diao, Y.; Shaw, L.; Bao, Z.; Mannsfeld, S. C. B. Morphology control strategies for solution-processed organic semiconductor thin films. *Energy Environ. Sci.* **2014**, *7*, 2145-2159.
13. Eslamian, M.; Zabihi, F. Ultrasonic substrate vibration-assisted drop casting (SVADC) for the fabrication of photovoltaic solar cell arrays and thin-film devices. *Nanoscale Res. Lett.* **2015**, *10*, 462-462.
14. Mampallil, D.; Eral, H. B. A review on suppression and utilization of the coffee-ring effect. *Adv. Colloid Interface Sci.* **2018**, *252*, 38-54.
15. Chen, L.-M.; Hong, Z.; Li, G.; Yang, Y. Recent progress in polymer solar cells: manipulation of polymer: fullerene morphology and the formation of efficient inverted polymer solar cells. *Adv.Mater.* **2009**, *21*, 1434-1449.
16. Chang, J.-F.; Sun, B.; Breiby, D. W.; Nielsen, M. M.; Sölling, T. I.; Giles, M.; McCulloch, I.; Sirringhaus, H. Enhanced mobility of poly(3-hexylthiophene) transistors by spin-coating from high-boiling-point solvents. *Chem. Mater.* **2004**, *16*, 4772-4776.

17. Ceratti, D. R.; Louis, B.; Paquez, X.; Faustini, M.; Grosso, D. A new dip coating method to obtain large-surface coatings with a minimum of solution. *Adv.Mater.* **2015**, *27*, 4958-4962.
18. Gaulding, E. A.; Diroll, B. T.; Goodwin, E. D.; Vrtis, Z. J.; Kagan, C. R.; Murray, C. B. Deposition of wafer-scale single-component and binary nanocrystal superlattice thin films *via* dip-coating. *Adv.Mater.* **2015**, *27*, 2846-2851.
19. Dey, M.; Doumenc, F.; Guerrier, B. Numerical simulation of dip-coating in the evaporative regime. *Eur. Phys. J. E* **2016**, *39*, 19.
20. Abdellah, A.; Fabel, B.; Lugli, P.; Scarpa, G. Spray deposition of organic semiconducting thin-films: towards the fabrication of arbitrary shaped organic electronic devices. *Org. Electron.* **2010**, *11*, 1031-1038.
21. Girotto, C.; Moia, D.; Rand, B. P.; Heremans, P. High-performance organic solar cells with spray-coated hole-transport and active layers. *Adv. Funct. Mater.* **2011**, *21*, 64-72.
22. Binda, M.; Natali, D.; Iacchetti, A.; Sampietro, M. Integration of an organic photodetector onto a plastic optical fiber by means of spray coating technique. *Adv.Mater.* **2013**, *25*, 4335-4339.
23. Blayo, A.; Pineaux, B. Printing processes and their potential for RFID printing. *Smart objects and ambient intelligence: innovative context-aware services: usages and technologies* **2005**, 27-30.
24. Hyun, W. J.; Secor, E. B.; Hersam, M. C.; Frisbie, C. D.; Francis, L. F. High-resolution patterning of graphene by screen printing with a silicon stencil for highly flexible printed electronics. *Adv.Mater.* **2015**, *27*, 109-115.
25. Pudas, M.; Hagberg, J.; Leppavuori, S. The absorption ink transfer mechanism of gravure offset printing for electronic circuitry. *IEEE Trans. Electron. Packag. Manuf.* **2002**, *25*, 335-343.
26. Sung, D.; Vornbrock, A. d. l. F.; Subramanian, V. Scaling and optimization of gravure-printed silver nanoparticle lines for printed electronics. *IEEE Trans. Compon. Packag. Technol.* **2010**, *33*, 105-114.
27. Lee, T.-M.; Lee, S.-H.; Noh, J.-H.; Kim, D.-S.; Chun, S. The effect of shear force on ink transfer in gravure offset printing. *J. Micromech. Microeng.* **2010**, *20*, 125026.
28. Cen, J.; Kitsomboonloha, R.; Subramanian, V. Cell filling in gravure printing for printed electronics. *Langmuir* **2014**, *30*, 13716-13726.
29. Sagu, J. S.; York, N.; Southee, D.; Wijayantha, K. Printed electrodes for flexible, light-weight solid-state supercapacitors–a feasibility study. *Circuit World* **2015**, *41*, 80-86.
30. Secor, E. B. Principles of aerosol jet printing. *Flexible and Printed Electronics* **2018**, *3*, 035002.
31. Binder, S.; Glatthaar, M.; Rädlein, E. Analytical investigation of aerosol jet printing. *Aerosol Sci. Technol.* **2014**, *48*, 924-929.
32. Cantù, E.; Tonello, S.; Abate, G.; Uberti, D.; Sardini, E.; Serpelloni, M. Aerosol jet printed 3D electrochemical sensors for protein detection. *Sensors* **2018**, *18*, 3719.
33. Mahajan, A.; Frisbie, C. D.; Francis, L. F. Optimization of aerosol jet printing for high-resolution, high-aspect ratio silver lines. *ACS Appl. Mater. Interfaces* **2013**, *5*, 4856-4864.
34. Singh, M.; Haverinen, H. M.; Dhagat, P.; Jabbour, G. E. Inkjet printing-process and its applications. *Adv.Mater.* **2010**, *22*, 673-685.
35. Derby, B. Inkjet printing of functional and structural materials: fluid property requirements, feature stability, and resolution. *Ann. Rev. Mater. Res.* **2010**, *40*, 395-414.

36. Liu, Y.-F.; Tsai, M.-H.; Pai, Y.-F.; Hwang, W.-S. Control of droplet formation by operating waveform for inks with various viscosities in piezoelectric inkjet printing. *Appl. Phys. A* **2013**, *111*, 509-516.
37. Shimoda, T.; Morii, K.; Seki, S.; Kiguchi, H. Inkjet printing of light-emitting polymer displays. *MRS Bulletin* **2003**, *28*, 821-827.
38. Khan, S.; Lorenzelli, L.; Dahiya, R. S. Technologies for printing sensors and electronics over large flexible substrates: a review. *IEEE Sensors J.* **2015**, *15*, 3164-3185.
39. Zardetto, V.; Brown, T. M.; Reale, A.; Di Carlo, A. Substrates for flexible electronics: a practical investigation on the electrical, film flexibility, optical, temperature, and solvent resistance properties. *J. Polym. Sci., Part B: Polym. Phys.* **2011**, *49*, 638-648.
40. MacDonald, W. A.; Looney, M. K.; MacKerron, D.; Eveson, R.; Adam, R.; Hashimoto, K.; Rakos, K. Latest advances in substrates for flexible electronics. *J. Soc. Inf. Display* **2007**, *15*, 1075-1083.
41. Garner, S.; Glaesemann, S.; Li, X. Ultra-slim flexible glass for roll-to-roll electronic device fabrication. *Appl. Phys. A* **2014**, *116*, 403-407.
42. Deus, C.; Salomon, J.; Wehner, U. Roll-to-roll coating of flexible glass. *Vakuum in Forschung und Praxis* **2016**, *28*, 40-44.
43. Schwamb, P.; Reusch, T. C.; Brabec, C. J., Flexible top-emitting OLEDs for lighting: bending limits. *SPIE* 2013, **8829**, 10.
44. Chen, F.; Wu, J.; Lee, C.; Huang, W.; Chen, H. P.; Chen, W. Flexible polymer photovoltaic devices prepared with inverted structures on metal foils. *IEEE Electron Dev. Lett.* **2009**, *30*, 727-729.
45. Chandra, A.; Takashima, M.; Li, J.; Beck, P.; Bruner, S.; Tinsley, D.; Sreenivasan, R.; Kamath, A. Considerations and methodology to determine R2R manufacturing and scaling of electronic devices on flexible stainless steel foil substrates. *MRS Advances* **2017**, *2*, 1029-1036.
46. Hübler, A.; Trnovec, B.; Zillger, T.; Ali, M.; Wetzold, N.; Mingebach, M.; Wagenpfahl, A.; Deibel, C.; Dyakonov, V. Printed paper photovoltaic cells. *Adv. Energy Mater.* **2011**, *1*, 1018-1022.
47. Kang, B. J.; Lee, C. K.; Oh, J. H. All-inkjet-printed electrical components and circuit fabrication on a plastic substrate. *Microelectron. Eng.* **2012**, *97*, 251-254.
48. Chang, J.; Zhang, X.; Ge, T.; Zhou, J. Fully printed electronics on flexible substrates: high gain amplifiers and DAC. *Org. Electron.* **2014**, *15*, 701-710.
49. MacDonald, W. A.; Looney, M. K.; MacKerron, D.; Eveson, R.; Rakos, K. Designing and manufacturing substrates for flexible electronics. *Plast. Rubber Compos.* **2008**, *37*, 41-45.
50. Yakimets, I.; MacKerron, D.; Giesen, P.; Kilmartin, K. J.; Goorhuis, M.; Meinders, E.; MacDonald, W. A., Polymer substrates for flexible electronics: Achievements and challenges. *Trans Tech Publ* **2010**.
51. Webb, A. J.; Szablewski, M.; Bloor, D.; Atkinson, D.; Graham, A.; Laughlin, P.; Lussey, D. A multi-component nanocomposite screen-printed ink with nonlinear touch sensitive electrical conductivity. *Nanotechnology* **2013**, *24*, 165501.
52. Larmagnac, A.; Eggenberger, S.; Janossy, H.; Vörös, J. Stretchable electronics based on Ag-PDMS composites. *Sci. Rep.* **2014**, *4*, 7254-7254.
53. Suzuki, M.; Takahashi, T.; Aoyagi, S. Flexible tactile sensor using polyurethane thin film. *Micromachines* **2012**, *3*, 315.
54. Cruz, S.; Rocha, L. A.; Viana, J. C. Enhanced printability of thermoplastic polyurethane substrates by silica particles surface interactions. *Appl. Surf. Sci.* **2016**, *360*, 198-206.

55. Lee, J.-W.; Yoo, Y.-T. A comparative study on dimensional stability of PET and BOPP substrates for fabrication of flexible electric/electronic devices through roll-to-roll printing. *J. Ind. Eng. Chem.* **2012**, *18*, 1647-1653.
56. van de Weijer, P.; Bouten, P. C. P.; Unnikrishnan, S.; Akkerman, H. B.; Michels, J. J.; van Mol, T. M. B. High-performance thin-film encapsulation for organic light-emitting diodes. *Org. Electron.* **2017**, *44*, 94-98.
57. Garner, S. M.; He, M.; Lo, P.; Sung, C.; Liu, C.; Hsieh, Y.; Hsu, R.; Ding, J.; Hu, J.; Chan, Y.; Lin, J.; Li, X.; Sorensen, M.; Li, J.; Cimo, P.; Kuo, C. Electrophoretic displays fabricated on ultra-slim flexible glass substrates. *J. Display Technol.* **2012**, *8*, 590-595.
58. Garner, S. M.; Lewis, S. C.; Chowdhury, D. Q. Flexible glass and its application for electronic devices. *24th International Workshop on Active-Matrix Flatpanel Displays and Devices (AM-FPD)* **2017**, 28-33.
59. Won, S. Poly Si TFT on microsheet. *Ecs Transactions* **2009**, *25*, 255-258.
60. Dragoman, M.; Flahaut, E.; Dragoman, D.; Al Ahmad, M.; Plana, R. Writing simple RF electronic devices on paper with carbon nanotube ink. *Nanotechnology* **2009**, *20*, 375203.
61. Hilder, M.; Winther-Jensen, B.; Clark, N. B. Paper-based, printed zinc–air battery. *J. Power Sources* **2009**, *194*, 1135-1141.
62. Zisman, W. A., Relation of the Equilibrium contact angle to liquid and solid constitution. *Advances in Chmeistry* **1964**, 43, 1-51.
63. Siau, S.; Vervaet, A.; Calster, A. V.; Swennen, I.; Schacht, E. Influence of wet chemical treatments on the evolution of epoxy polymer layer surface roughness for use as a build-up layer. *Appl. Surf. Sci.* **2004**, *237*, 457-462.
64. Strobel, M.; Jones, V.; Lyons, C. S.; Ulsh, M.; Kushner, M. J.; Dorai, R.; Branch, M. C. A comparison of corona-treated and flame-treated polypropylene films. *Plasmas Polym.* **2003**, *8*, 61-95.
65. Morent, R.; De Geyter, N.; Leys, C. Effects of operating parameters on plasma-induced PET surface treatment. *Nucl. Instrum. Methods Phys. Res. B* **2008**, *266*, 3081-3085.
66. McDonald, J. C.; Whitesides, G. M. Poly(dimethylsiloxane) as a material for fabricating microfluidic devices. *Acc. Chem. Res.* **2002**, *35*, 491-499.
67. Cammarano, A.; De Luca, G.; Amendola, E. Surface modification and adhesion improvement of polyester films. *Cent. Eur. J. Chem.* **2013**, *11*, 35-45.
68. Kim, M.-G.; Kanatzidis, M. G.; Facchetti, A.; Marks, T. J. Low-temperature fabrication of high-performance metal oxide thin-film electronics via combustion processing. *Nature Mater.* **2011**, *10*, 382.
69. Kim, S. H.; Hong, K.; Xie, W.; Lee, K. H.; Zhang, S.; Lodge, T. P.; Frisbie, C. D. Electrolyte-gated transistors for organic and printed electronics. *Adv.Mater.* **2013**, *25*, 1822-1846.
70. Plummer, J. D., Silicon VLSI technology: fundamentals, practice and modeling. *Pearson Education India* **2009**.
71. Kamyshny, A.; Steinke, J.; Magdassi, S. Metal-based inkjet inks for printed electronics. *The Open Applied Physics Journal* **2011**, *4*.
72. Wang, X.; Liu, J. Recent Advancements in liquid metal flexible printed electronics: properties, technologies, and applications. *Micromachines* **2016**, *7*, 206.
73. Grouchko, M.; Kamyshny, A.; Mihailescu, C. F.; Anghel, D. F.; Magdassi, S. Conductive inks with a "built-in" mechanism that enables sintering at room temperature. *ACS Nano* **2011**, *5*, 3354-3359.
74. Dong, Y.; Lin, Z.; Li, X.; Zhu, Q.; Li, J.-G.; Sun, X. A low temperature and air-sinterable copper–diamine complex-based metal organic decomposition ink for printed electronics. *J. Mater. Chem. C* **2018**, *6*, 6406-6415.

75. Moisala, A.; Nasibulin, A. G.; Kauppinen, E. I. The role of metal nanoparticles in the catalytic production of single-walled carbon nanotubes-a review. *J. Phys.: Condens. Matter* **2003**, *15*, S3011-S3035.
76. Lee, Y.; Choi, J.-r.; Lee, K. J.; Stott, N. E.; Kim, D. Large-scale synthesis of copper nanoparticles by chemically controlled reduction for applications of inkjet-printed electronics. *Nanotechnology* **2008**, *19*, 415604.
77. Kosmala, A.; Wright, R.; Zhang, Q.; Kirby, P. Synthesis of silver nano particles and fabrication of aqueous Ag inks for inkjet printing. *Mater. Chem. Phys.* **2011**, *129*, 1075-1080.
78. R, V. K. R.; K, V. A.; P. S, K.; Singh, S. P. Conductive silver inks and their applications in printed and flexible electronics. *RSC Adv.* **2015**, *5*, 77760-77790.
79. Rajan, K.; Roppolo, I.; Chiappone, A.; Bocchini, S.; Perrone, D.; Chiolerio, A. Silver nanoparticle ink technology: state of the art. *Nanotechnol. Sci. Appl.* **2016**, *9*, 1-13.
80. Abhinav K, V.; Rao R, V. K.; Karthik, P. S.; Singh, S. P. Copper conductive inks: synthesis and utilization in flexible electronics. *RSC Adv.* **2015**, *5*, 63985-64030.
81. Jeong, S.; Lee, S. H.; Jo, Y.; Lee, S. S.; Seo, Y.-H.; Ahn, B. W.; Kim, G.; Jang, G.-E.; Park, J.-U.; Ryu, B.-H.; Choi, Y. Air-stable, surface-oxide free Cu nanoparticles for highly conductive Cu ink and their application to printed graphene transistors. *J. Mater. Chem. C* **2013**, *1*, 2704-2710.
82. Li, N.; Zhao, P.; Astruc, D. Anisotropic gold nanoparticles: synthesis, properties, applications, and toxicity. *Angew. Chem. Int. Ed.* **2014**, *53*, 1756-1789.
83. Tamburri, E.; Angjellari, M.; Tomellini, M.; Gay, S.; Reina, G.; Lavecchia, T.; Barbini, P.; Pasquali, M.; Orlanducci, S. Electrochemical growth of nickel nanoparticles on carbon nanotubes fibers: kinetic modeling and implications for an easy to handle platform for gas sensing device. *Electrochim. Acta* **2015**, *157*, 115-124.
84. Green, M. Organometallic based strategies for metal nanocrystal synthesis. *Chem. Commun.* **2005**, 3002-3011.
85. Herman, D. A. J.; Cheong-Tilley, S.; McGrath, A. J.; McVey, B. F. P.; Lein, M.; Tilley, R. D. How to choose a precursor for decomposition solution-phase synthesis: the case of iron nanoparticles. *Nanoscale* **2015**, *7*, 5951-5954.
86. Iravani, S.; Korbekandi, H.; Mirmohammadi, S. V.; Zolfaghari, B. Synthesis of silver nanoparticles: chemical, physical and biological methods. *Res. Pharm. Sci.* **2014**, *9*, 385-406.
87. Dang, M. C.; Dung Dang, T. M.; Fribourg-Blanc, E. Inkjet printing technology and conductive inks synthesis for microfabrication techniques. *Adv. Nat. Sci.: Nanosci. Nanotechnol* **2013**, *4*, 015009.
88. Matsuzaki, R.; Tabayashi, K. Highly stretchable, global, and distributed local strain sensing line using GaInSn electrodes for wearable electronics. *Adv. Funct. Mater.* **2015**, *25*, 3806-3813.
89. Vacca, A.; Mascia, M.; Rizzardini, S.; Corgiolu, S.; Palmas, S.; Demelas, M.; Bonfiglio, A.; Ricci, P. C. Preparation and characterisation of transparent and flexible PEDOT:PSS/PANI electrodes by ink-jet printing and electropolymerisation. *RSC Adv.* **2015**, *5*, 79600-79606.
90. Clemens, W.; Fix, W.; Ficker, J.; Knobloch, A.; Ullmann, A. From polymer transistors toward printed electronics. *J. Mater. Res.* **2011**, *19*, 1963-1973.
91. Chiang, C. K.; Fincher, C. R.; Park, Y. W.; Heeger, A. J.; Shirakawa, H.; Louis, E. J.; Gau, S. C.; MacDiarmid, A. G. Electrical conductivity in doped polyacetylene. *Phys. Rev. Lett.* **1977**, *39*, 1098-1101.

92. Chen, S.-P.; Chiu, H.-L.; Wang, P.-H.; Liao, Y.-C. Inkjet printed conductive tracks for printed electronics. *ECS J. Solid State Sci. Technol.* **2015**, *4*, P3026-P3033.
93. Baker, C. O.; Huang, X.; Nelson, W.; Kaner, R. B. Polyaniline nanofibers: broadening applications for conducting polymers. *Chem. Soc. Rev.* **2017**, *46*, 1510-1525.
94. Mabrook, M. F.; Pearson, C.; Petty, M. C. Inkjet-printed polypyrrole thin films for vapour sensing. *Sens. Actuators, B* **2006**, *115*, 547-551.
95. Kamyshny, A.; Magdassi, S. Conductive nanomaterials for printed electronics. *Small* **2014**, *10*, 3515-3535.
96. Hecht, D. S.; Hu, L.; Irvin, G. Emerging transparent electrodes based on thin films of carbon nanotubes, graphene, and metallic nanostructures. *Adv.Mater.* **2011**, *23*, 1482-1513.
97. De Volder, M. F. L.; Tawfick, S. H.; Baughman, R. H.; Hart, A. J. Carbon nanotubes: present and future commercial applications. *Science* **2013**, *339*, 535.
98. Lee, C.; Wei, X.; Kysar, J. W.; Hone, J. Measurement of the elastic properties and intrinsic strength of monolayer graphene. *Science* **2008**, *321*, 385.
99. Tortorich, R. P.; Choi, J.-W. Inkjet printing of carbon nanotubes. *Nanomaterials (Basel, Switzerland)* **2013**, *3*, 453-468.
100. Shimoni, A.; Azoubel, S.; Magdassi, S. Inkjet printing of flexible high-performance carbon nanotube transparent conductive films by "coffee ring effect". *Nanoscale* **2014**, *6*, 11084-11089.
101. Geim, A. K. Graphene: status and prospects. *Science* **2009**, *324*, 1530.
102. Balandin, A. A.; Ghosh, S.; Bao, W.; Calizo, I.; Teweldebrhan, D.; Miao, F.; Lau, C. N. Superior thermal conductivity of single-layer graphene. *Nano Lett.* **2008**, *8*, 902-907.
103. Liu, C.; Yu, Z.; Neff, D.; Zhamu, A.; Jang, B. Z. Graphene-based supercapacitor with an ultrahigh energy density. *Nano Lett.* **2010**, *10*, 4863-4868.
104. Lin, Y.-M.; Jenkins, K. A.; Valdes-Garcia, A.; Small, J. P.; Farmer, D. B.; Avouris, P. Operation of graphene transistors at gigahertz frequencies. *Nano Lett.* **2009**, *9*, 422-426.
105. Huang, L.; Huang, Y.; Liang, J.; Wan, X.; Chen, Y. Graphene-based conducting inks for direct inkjet printing of flexible conductive patterns and their applications in electric circuits and chemical sensors. *Nano Res.* **2011**, *4*, 675-684.
106. Li, X.; Zhang, G.; Bai, X.; Sun, X.; Wang, X.; Wang, E.; Dai, H. Highly conducting graphene sheets and Langmuir–Blodgett films. *Nature Nanotech.* **2008**, *3*, 538.
107. Bae, S.; Kim, H.; Lee, Y.; Xu, X.; Park, J.-S.; Zheng, Y.; Balakrishnan, J.; Lei, T.; Ri Kim, H.; Song, Y. I.; Kim, Y.-J.; Kim, K. S.; Özyilmaz, B.; Ahn, J.-H.; Hong, B. H.; Iijima, S. Roll-to-roll production of 30-inch graphene films for transparent electrodes. *Nature Nanotech.* **2010**, *5*, 574.
108. Li, X.; Cai, W.; An, J.; Kim, S.; Nah, J.; Yang, D.; Piner, R.; Velamakanni, A.; Jung, I.; Tutuc, E.; Banerjee, S. K.; Colombo, L.; Ruoff, R. S. Large-area synthesis of high-quality and uniform graphene films on copper foils. *Science* **2009**, *324*, 1312.
109. Novoselov, K. S.; Fal'ko, V. I.; Colombo, L.; Gellert, P. R.; Schwab, M. G.; Kim, K. A roadmap for graphene. *Nature* **2012**, *490*, 192.
110. Paton, K. R.; Varrla, E.; Backes, C.; Smith, R. J.; Khan, U.; O'Neill, A.; Boland, C.; Lotya, M.; Istrate, O. M.; King, P.; Higgins, T.; Barwich, S.; May, P.; Puczkarski, P.; Ahmed, I.; Moebius, M.; Pettersson, H.; Long, E.; Coelho, J.; O'Brien, S. E.; McGuire, E. K.; Sanchez, B. M.; Duesberg, G. S.; McEvoy, N.; Pennycook, T. J.; Downing, C.; Crossley, A.; Nicolosi, V.; Coleman, J. N. Scal-

able production of large quantities of defect-free few-layer graphene by shear exfoliation in liquids. *Nature Mater.* **2014**, *13*, 624.
111. Hernandez, Y.; Nicolosi, V.; Lotya, M.; Blighe, F. M.; Sun, Z.; De, S.; McGovern, I. T.; Holland, B.; Byrne, M.; Gun'Ko, Y. K.; Boland, J. J.; Niraj, P.; Duesberg, G.; Krishnamurthy, S.; Goodhue, R.; Hutchison, J.; Scardaci, V.; Ferrari, A. C.; Coleman, J. N. High-yield production of graphene by liquid-phase exfoliation of graphite. *Nature Nanotech.* **2008**, *3*, 563.
112. Schniepp, H. C.; Li, J.-L.; McAllister, M. J.; Sai, H.; Herrera-Alonso, M.; Adamson, D. H.; Prud'homme, R. K.; Car, R.; Saville, D. A.; Aksay, I. A. Functionalized single graphene sheets derived from splitting graphite oxide. *J. Phys. Chem. B* **2006**, *110*, 8535-8539.
113. Virojanadara, C.; Syväjarvi, M.; Yakimova, R.; Johansson, L. I.; Zakharov, A. A.; Balasubramanian, T. Homogeneous large-area graphene layer growth on 6H-SiC(0001). *Phys. Rev. B* **2008**, *78*, 245403.
114. Riedl, C.; Coletti, C.; Starke, U. Structural and electronic properties of epitaxial graphene on SiC(0001): a review of growth, characterization, transfer doping and hydrogen intercalation. *J. Phys. D: Appl. Phys.* **2010**, *43*, 374009.
115. Cummins, G.; Desmulliez, M. P. Inkjet printing of conductive materials: a review. *Circuit world* **2012**, *38*, 193-213.
116. Johnson, D. W.; Dobson, B. P.; Coleman, K. S. A manufacturing perspective on graphene dispersions. *Curr. Opin. Colloid Interface Sci.* **2015**, *20*, 367-382.
117. Torrisi, F.; Hasan, T.; Wu, W.; Sun, Z.; Lombardo, A.; Kulmala, T. S.; Hsieh, G.-W.; Jung, S.; Bonaccorso, F.; Paul, P. J.; Chu, D.; Ferrari, A. C. Inkjet-printed graphene electronics. *ACS Nano* **2012**, *6*, 2992-3006.
118. Secor, E. B.; Prabhumirashi, P. L.; Puntambekar, K.; Geier, M. L.; Hersam, M. C. Inkjet printing of high conductivity, flexible graphene patterns. *J. Phys. Chem. Lett.* **2013**, *4*, 1347-1351.
119. Arapov, K.; Rubingh, E.; Abbel, R.; Laven, J.; de With, G.; Friedrich, H. Conductive screen printing inks by gelation of graphene dispersions. *Adv. Funct. Mater.* **2016**, *26*, 586-593.
120. Mohan, V. B.; Lau, K.-t.; Hui, D.; Bhattacharyya, D. Graphene-based materials and their composites: a review on production, applications and product limitations. *Compos. B Eng.* **2018**, *142*, 200-220.
121. Yang, W.; Wang, C. Graphene and the related conductive inks for flexible electronics. *J. Mater. Chem. C* **2016**, *4*, 7193-7207.
122. Li, L.; Guo, Y.; Zhang, X.; Song, Y. Inkjet-printed highly conductive transparent patterns with water based Ag-doped graphene. *J. Mater. Chem. A* **2014**, *2*, 19095-19101.
123. Wang, G.; Wang, Z.; Liu, Z.; Xue, J.; Xin, G.; Yu, Q.; Lian, J.; Chen, M. Y. Annealed graphene sheets decorated with silver nanoparticles for inkjet printing. *Chem. Eng. J.* **2015**, *260*, 582-589.
124. Xu, L. Y.; Yang, G. Y.; Jing, H. Y.; Wei, J.; Han, Y. D. Ag–graphene hybrid conductive ink for writing electronics. *Nanotechnology* **2014**, *25*, 055201.
125. Zhang, W.; Bi, E.; Li, M.; Gao, L. Synthesis of Ag/rGO composite as effective conductive ink filler for flexible inkjet printing electronics. *Colloid Surf. A-Physicochem. Eng. Asp.* **2016**, *490*, 232-240.
126. Hu, Z.; Tong, G.; Lin, D.; Chen, C.; Guo, H.; Xu, J.; Zhou, L. Graphene-reinforced metal matrix nanocomposites–a review. *Mater. Sci. Technol.* **2016**, *32*, 930-953.
127. Utomo, A. T.; Baker, M.; Pacek, A. W. Flow pattern, periodicity and energy dissipation in a batch rotor–stator mixer. *Chem. Eng. Res. Des.* **2008**, *86*, 1397-1409.

128. Chen, X.; Dobson, J. F.; Raston, C. L. Vortex fluidic exfoliation of graphite and boron nitride. *Chem. Commun.* **2012**, *48*, 3703-3705.
129. Walker, S. B.; Lewis, J. A. Reactive silver inks for patterning high-conductivity features at mild temperatures. *J. Am. Chem. Soc.* **2012**, *134*, 1419-1421.
130. Lawson, A. Factors influencing the compensation effect during formic acid decomposition on silver. *J. Catal.* **1968**, *11*, 295-304.
131. Schlesinger, M.; Paunovic, M., Modern electroplating. *John Wiley & Sons* **2011**, 55.
132. Vargo, T. G.; Gardella, J. A.; Calvert, J. M.; Chen, M.-S. Adhesive electroless metallization of fluoropolymeric substrates. *Science* **1993**, *262*, 1711-1712.
133. Dugasz, J.; Szász, A. Factors affecting the adhesion of electroless coatings. *Surf. Coat. Technol.* **1993**, *58*, 57-62.
134. Azzaroni, O.; Zheng, Z.; Yang, Z.; Huck, W. T. Polyelectrolyte brushes as efficient ultrathin platforms for site-selective copper electroless deposition. *Langmuir* **2006**, *22*, 6730-6733.
135. Djokić, S. S.; Cavallotti, P. L., Electroless deposition: theory and applications. *Springer New York* **2010**, 251-289.
136. Smits, F. M. Measurement of sheet resistivities with the four-point probe. *Bell Syst. Tech. J.* **1958**, *37*, 711-718.
137. Weller, R. A. An algorithm for computing linear four-point probe thickness correction factors. *Rev. Sci. Instrum.* **2001**, *72*, 3580-3586.
138. Mizusaki, J.; Waragai, K.; Tsuchiya, S.; Tagawa, H.; Arai, Y.; Kuwayama, Y. Simple mathematical model for the electrical conductivity of highly porous ceramics. *J. Am. Ceram. Soc.* **1996**, *79*, 109-113.
139. Juretschke, H. J.; Landauer, R.; Swanson, J. A. Hall effect and conductivity in porous media. *J. Appl. Phys.* **1956**, *27*, 838-839.
140. Zhao, J.; Zeng, S.; Wu, B.; Zhang, S.-L.; Zhang, Z.-B. Re-organized graphene nanoplatelet thin films achieved by a two-step hydraulic method. *Diamond Relat. Mater.* **2018**, *84*, 141-145.
141. Shacham-Diamand, Y.; Dubin, V. M. Copper electroless deposition technology for ultra-large-scale-integration (ULSI) metallization. *Microelectron. Eng.* **1997**, *33*, 47-58.
142. Xu, L.; Liao, J.; Huang, L.; Ou, D.; Guo, Z.; Zhang, H.; Ge, C.; Gu, N.; Liu, J. Surface-bound nanoparticles for initiating metal deposition. *Thin Solid Films* **2003**, *434*, 121-125.
143. Zhao, J.; Wen, C.; Sun, R.; Zhang, S.-L.; Wu, B.; Zhang, Z.-B. A sequential process of graphene exfoliation and site-selective copper/graphene metallization enabled by multifunctional 1-pyrenebutyric acid tetrabutylammonium salt. *ACS Appl. Mater. Interfaces* **2019**, *11*, 6448-6455.
144. Subramaniam, C.; Yamada, T.; Kobashi, K.; Sekiguchi, A.; Futaba, D. N.; Yumura, M.; Hata, K. One hundred fold increase in current carrying capacity in a carbon nanotube–copper composite. *Nat. Commun.* **2013**, *4*, 2202.
145. Kang, H.; Jung, S.; Jeong, S.; Kim, G.; Lee, K. Polymer-metal hybrid transparent electrodes for flexible electronics. *Nat. Commun.* **2015**, *6*, 6503.
146. Lee, H. M.; Choi, S.-Y.; Jung, A.; Ko, S. H. Highly Conductive aluminum textile and paper for flexible and wearable electronics. *Angew. Chem. Int. Ed.* **2013**, *52*, 7718-7723.
147. Russo, A.; Ahn, B. Y.; Adams, J. J.; Duoss, E. B.; Bernhard, J. T.; Lewis, J. A. Pen-on-paper flexible electronics. *Adv.Mater.* **2011**, *23*, 3426-3430.
148. Hösel, M.; Krebs, F. C. Large-scale roll-to-roll photonic sintering of flexo printed silver nanoparticle electrodes. *J. Mater. Chem.* **2012**, *22*, 15683-15688.

149. Zhao, J.; Song, M.; Wen, C.; Majee, S.; Yang, D.; Wu, B.; Zhang, S.-L.; Zhang, Z.-B. Microstructure-tunable highly conductive graphene–metal composites achieved by inkjet printing and low temperature annealing. *J. Micromech. Microeng.* **2018**, *28*, 035006.
150. Wu, Z.-S.; Yang, S.; Sun, Y.; Parvez, K.; Feng, X.; Müllen, K. 3D nitrogen-doped graphene aerogel-supported Fe_3O_4 nanoparticles as efficient electrocatalysts for the oxygen reduction reaction. *J. Am. Chem. Soc.* **2012**, *134*, 9082-9085.
151. Wu, T.; Chen, M.; Zhang, L.; Xu, X.; Liu, Y.; Yan, J.; Wang, W.; Gao, J. Three-dimensional graphene-based aerogels prepared by a self-assembly process and its excellent catalytic and absorbing performance. *J. Mater. Chem. A* **2013**, *1*, 7612-7621.
152. Wu, J.; Tao, K.; Zhang, J.; Guo, Y.; Miao, J.; Norford, L. K. Chemically functionalized 3D graphene hydrogel for high performance gas sensing. *J. Mater. Chem. A* **2016**, *4*, 8130-8140.
153. Shen, Y.; Zhu, X.; Zhu, L.; Chen, B. Synergistic effects of 2D graphene oxide nanosheets and 1D carbon nanotubes in the constructed 3D carbon aerogel for high performance pollutant removal. *Chem. Eng. J.* **2017**, *314*, 336-346.
154. Wu, Z.-S.; Winter, A.; Chen, L.; Sun, Y.; Turchanin, A.; Feng, X.; Müllen, K. Three-dimensional nitrogen and boron co-doped graphene for high-performance all-solid-state supercapacitors. *Adv.Mater.* **2012**, *24*, 5130-5135.
155. Gorgolis, G.; Galiotis, C. Graphene aerogels: a review. *2D Materials* **2017**, *4*, 032001.
156. Giri, S. D.; Sarkar, A. Electrochemical study of bulk and monolayer copper in alkaline solution. *J. Electrochem. Soc.* **2016**, *163*, H252-H259.
157. Zhao, J.; Pan, R.; Sun, R.; Wen, C.; Zhang, S.-L.; Wu, B.; Nyholm, L.; Zhang, Z.-B. High-conductivity reduced-graphene-oxide/copper aerogel for energy storage. *Nano Energy* **2019**, *60*, 760-767.

Acta Universitatis Upsaliensis

Digital Comprehensive Summaries of Uppsala Dissertations from the Faculty of Science and Technology 1799

Editor: The Dean of the Faculty of Science and Technology

A doctoral dissertation from the Faculty of Science and Technology, Uppsala University, is usually a summary of a number of papers. A few copies of the complete dissertation are kept at major Swedish research libraries, while the summary alone is distributed internationally through the series Digital Comprehensive Summaries of Uppsala Dissertations from the Faculty of Science and Technology. (Prior to January, 2005, the series was published under the title "Comprehensive Summaries of Uppsala Dissertations from the Faculty of Science and Technology".)

Distribution: publications.uu.se
urn:nbn:se:uu:diva-381348

ACTA
UNIVERSITATIS
UPSALIENSIS
UPPSALA
2019